ThermoFAST: A new tool for predicting solids formation risk in cryogenic gas processing

Corey Baker[1], Arman Siahvashi[1], Jordan Oakley[1], Thomas Hughes[2], Darren Rowland[1], Stanley Huang[3] and Eric F. May[1]

1. *Fluid Science & Resources Division, School of Mechanical and Chemical Engineering, The University of Western Australia, 35 Stirling Hwy, Crawley 6009, AUSTRALIA*
2. *Oil & Gas Engineering, Monash University, Clayton VIC, AUSTRALIA*
3. *Chevron Energy Technology Company, Houston TX 77002, USA*

The formation and deposition of solids during the cryogenic processing of natural gas is a perennial risk for operators. While several tools are available for predicting the temperatures at which heavy hydrocarbon solids will form in cryogenic processing equipment, the Kohn and Luks Solids Solubility Program (KLSSP) from GPA Midstream has become an industry standard. However, although it describes well many of the data sets generated as part of the GPA's research program in the 1970s and 1980s, it suffers from limitations including fixed ranges of temperature, mixture composition, and no dependence on pressure. Furthermore, the available software implementations of KLSSP are not optimised for modern computers. We present here a new software tool called ThermoFAST, which overcomes these limitations and has been endorsed by GPA Midstream recently to replace the KLSSP. ThermoFAST uses a cubic equation of state which is capable of rapidly calculating solid-liquid, solid-vapor, and solid-liquid-vapor equilibrium conditions in addition to normal vapor-liquid phase envelopes. The ThermoFAST model has been tuned to binary mixture data from both the GPA and other literature sources, and thoroughly tested against solids formation data for multicomponent LNG mixtures; this includes the formation of solid CO_2 over a wide range of operating conditions. We will also describe our ongoing program to advance the industry's knowledge of cryogenic solids formation risk through the acquisition of new data for systems that have not been adequately studied in the past such as p-xylene in binary mixtures with methane or ethane.

ThermoFAST [GPA] Download: https://gpamidstream.org/committees/research

Table of Contents

1 Introduction

Natural gas accounts for nearly 22 % of world energy production [1], with approximately 32 % of global trade occurring through the production and transport of Liquefied Natural Gas (LNG) [2]. Prior to liquefaction, several stages of processing are undertaken to reduce the amounts of impurities (acid gases, water, heavy hydrocarbons) in the gas stream to acceptable levels. The methane-rich gas stream is cooled to about 120 K (-244 °F) in the main cryogenic heat exchanger (MCHE). Due to the very low temperatures in the MCHE, the formation and deposition of solids during the cryogenic processing of natural gas is a perennial risk for operators. Failure to reduce the fractions of impurities below their respective solubility limits in LNG poses a significant risk of blockage in the MCHE, which can require time-consuming and expensive actions to remediate [3]. For this reason, an accurate knowledge of, and an ability to predict the solubility of impurities in LNG is highly important.

The foremost tool used in industry for predicting the solubility of hydrocarbon solids in cryogenic fluids is the Kohn and Luks Solids Solubility Program (KLSSP) from GPA Midstream (Figure 1.1).

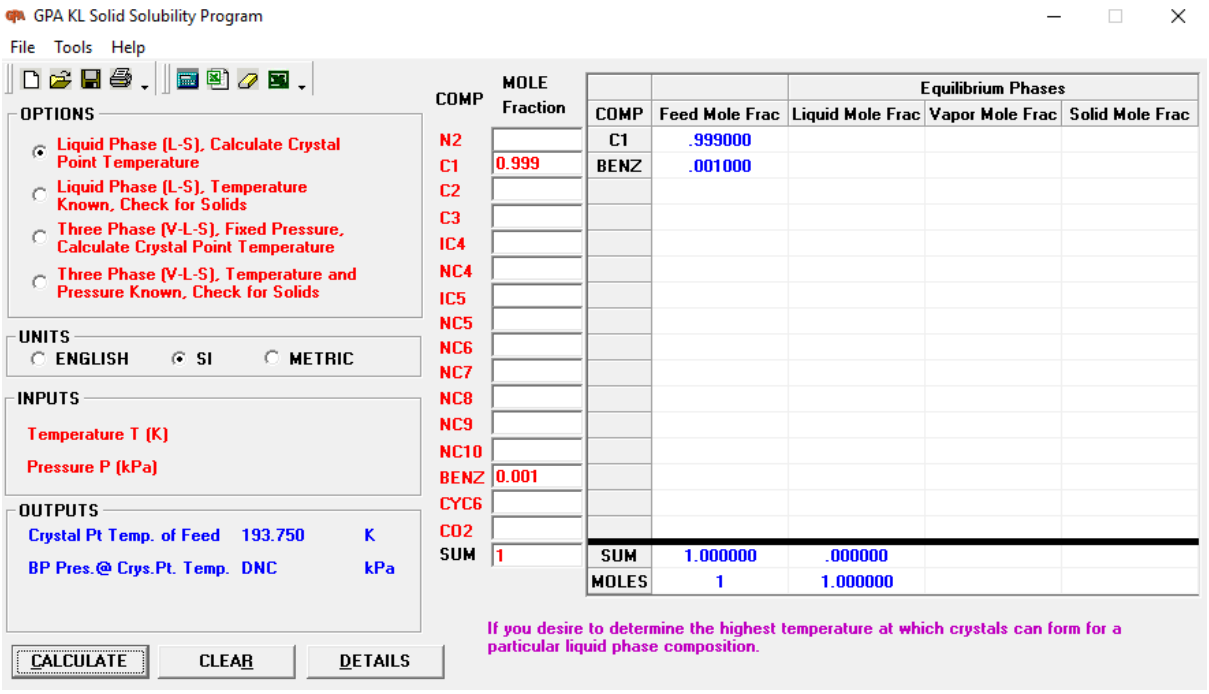

Figure 1.1: The user interface of the Kohn and Luks Solids Solubility Program (KLSSP) from GPA Midstream.

This tool uses empirical functions based on activity coefficient models to reproduce closely certain experimental solubility data, especially those resulting from the extensive campaign

headed by Kohn and Luks under the direction of GPA during the 1970s and '80s [4-18]. Unfortunately, several limitations of KLSSP limit the viability of its future use. First, the empirical activity coefficient model employed in KLSSP contains no dependence on pressure. Second, the model inputs are narrowly restricted in terms of temperature (> 100 K), available components and maximum composition of impurities (Table 1.1). Third, the software can only determine a single solid-fluid equilibrium condition: as discussed below, more than one solid formation temperature can exist for mixtures. Finally, the software often requires excessive computation times and is not well-suited to modern computers.

Table 1.1: Components available in KLSSP and their maximum mole fractions within its model. Temperatures are restricted to greater than 100 K.

Component	***Range of Validity*** */ mol mol^{-1}*	***Component***	***Range of Validity*** */ mol mol^{-1}*
Nitrogen	< 1.0	*n-Hexane*	< 0.2
Methane	< 1.0	*n-Heptane*	< 0.05
Ethane	< 1.0	*n-Octane*	< 0.05
Propane	< 1.0	*n-Nonane*	< 0.1
i-Butane	< 0.4	*n-Decane*	< 0.3
n-Butane	< 0.4	*Benzene*	< 0.001
i-Pentane	< 0.3	*Cyclohexane*	< 0.05
n-Pentane	< 0.3	*Carbon Dioxide*	< 0.15

Presented here is a new software tool called ThermoFAST, which has been designed to overcome the main limitations of KLSSP. ThermoFAST has been tested over wide ranges of pressure, temperature and fluid composition. Due to its success at predicting solids formation including heavy hydrocarbons and CO_2, ThermoFAST has been endorsed recently by GPA Midstream to replace KLSSP. The following sections describe ThermoFAST's User Interface (UI), thermodynamic model development and comparisons between experimental data for binary and multicomponent fluid systems.

2 ThermoFAST: A New Software Tool for Cryogenic Processing

ThermoFAST is a thermodynamic calculator for LNG and natural gas capable of calculating vapour-liquid-solid equilibria, predicting solids formation in complex multicomponent systems, and generating full phase envelopes as well as solubility curves. ThermoFAST is a

product of the Fluid Science & Resources group at the University of Western Australia, funded through the ARC Training Centre for LNG Futures. Although the GPA Midstream Association did not fund nor direct its development and does not claim ownership of the software, individual members of the GPA Midstream Association Research Committee reviewed ThermoFAST during its development. The consensus view of the Research Committee members was that the software could become a valuable predictive tool in industry; certain suggestions were made to improve the UI to help achieve this outcome.

ThermoFAST-GPA 1.1 was completed on 30th December 2017 and is the version of ThermoFAST recommended by the GPA Midstream Association Research Committee for use by GPA Midstream members. Its UI was designed to deliver a simplified work flow for the user. The four main tabs are (1) FLUID, (2) COMPOSITION, (3) FLASH and (4) SOLIDS. The user supplies information to each tab in order, where a range of calculations are available. Other tasks such as model and unit definition and saving/loading are performed via the upper menu bar. A brief overview on how to use the software follows; more detail can be found through the User Manual available under the "Help" option in the ThermoFAST menu.

2.1 FLUID

ThermoFAST opens first on the FLUID tab (Figure 2.1).

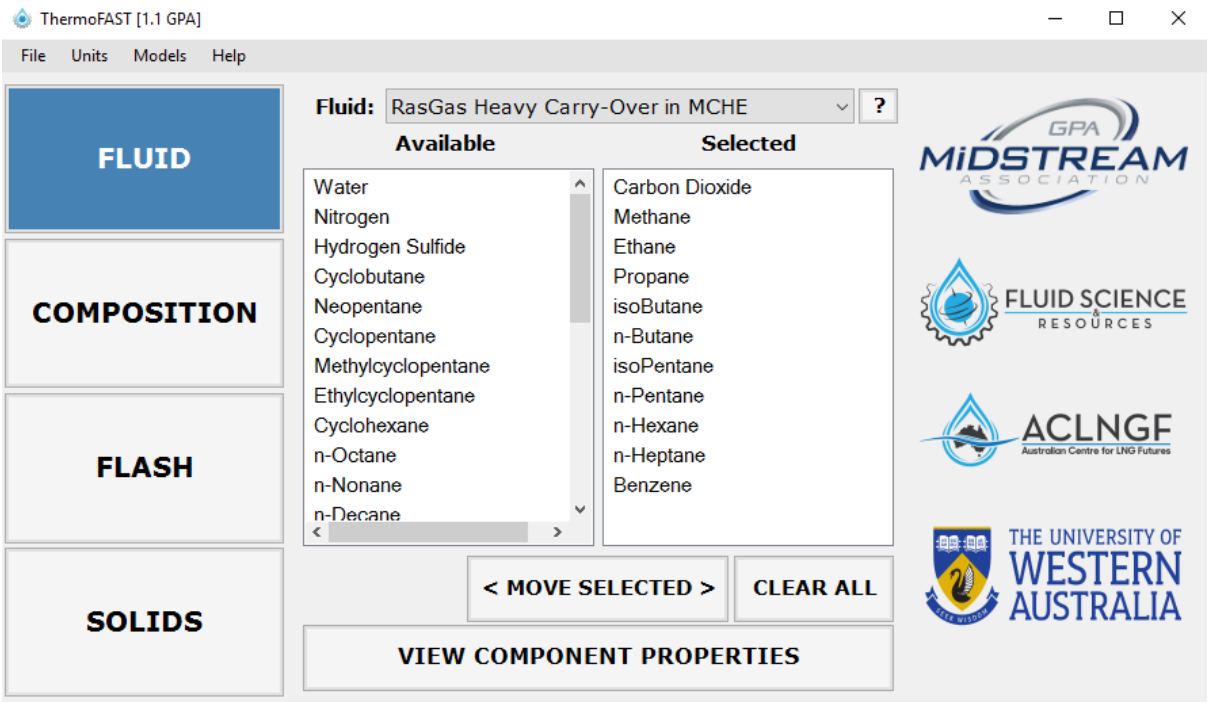

Figure 2.1: ThermoFAST-GPA user-interface showing the "FLUID" tab. The "RasGas Heavy Carry-Over in MCHE" mixture is described by Baker et al. (2018) [3].

The user defines a fluid mixture (or selects one saved previously) from the 37 natural gas components included in the software. The properties of each component including normal melting and critical temperatures may be viewed at this stage. The gas mixture shown in Figure 2.1 and Figure 2.2 is from Baker et al. (2018) [3]; in that paper ThermoFAST was used to analyse an industrial solid formation incident that occurred in the RasGas plant.

2.2 COMPOSITION

The COMPOSITION tab (Figure 2.2) allows the user to define multiple sets of compositions for the set of components selected in the FLUID tab. The program is able to save or load previous composition sets, handle the specification of fractions equal to zero, and warn users of non-normalisation to eliminate user error when entering compositions. The user can also view the VLE phase envelope of a specific mixture (Figure 2.3) and copy its data over to Excel.

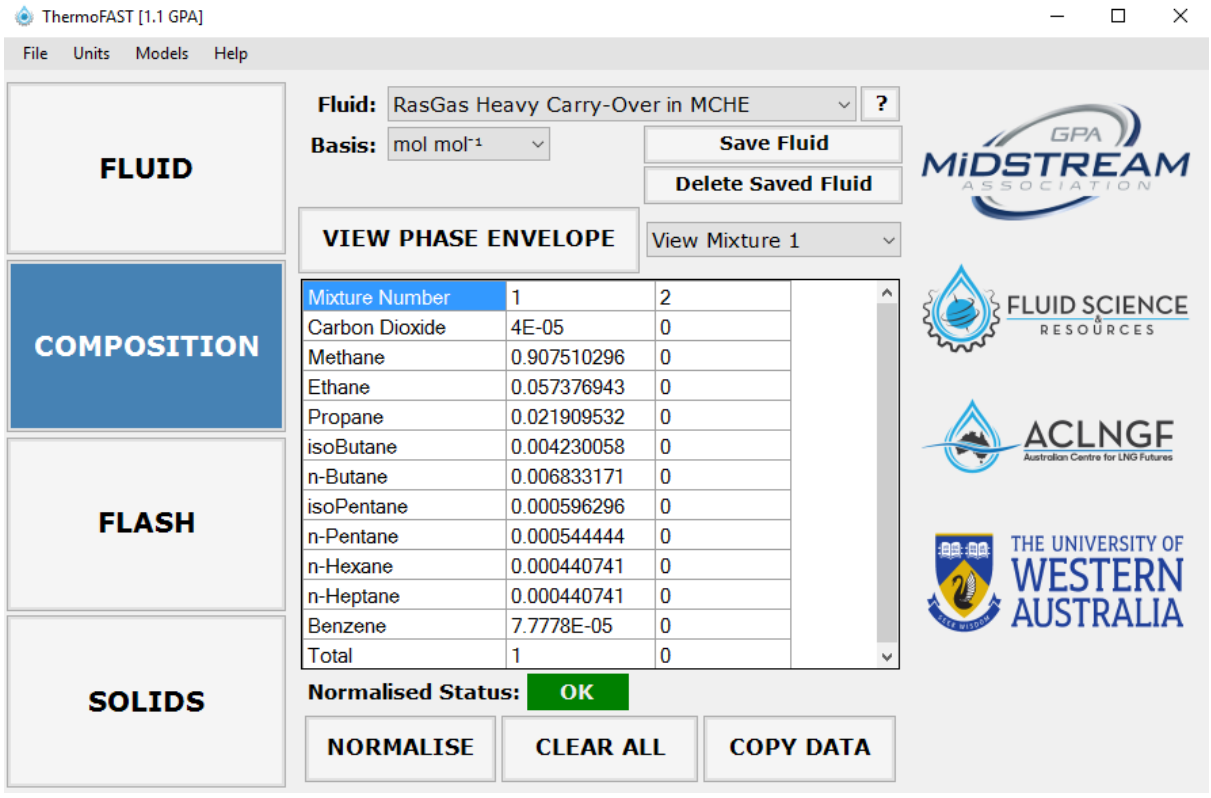

Figure 2.2: ThermoFAST-GPA user-interface showing the "COMPOSITION" tab.

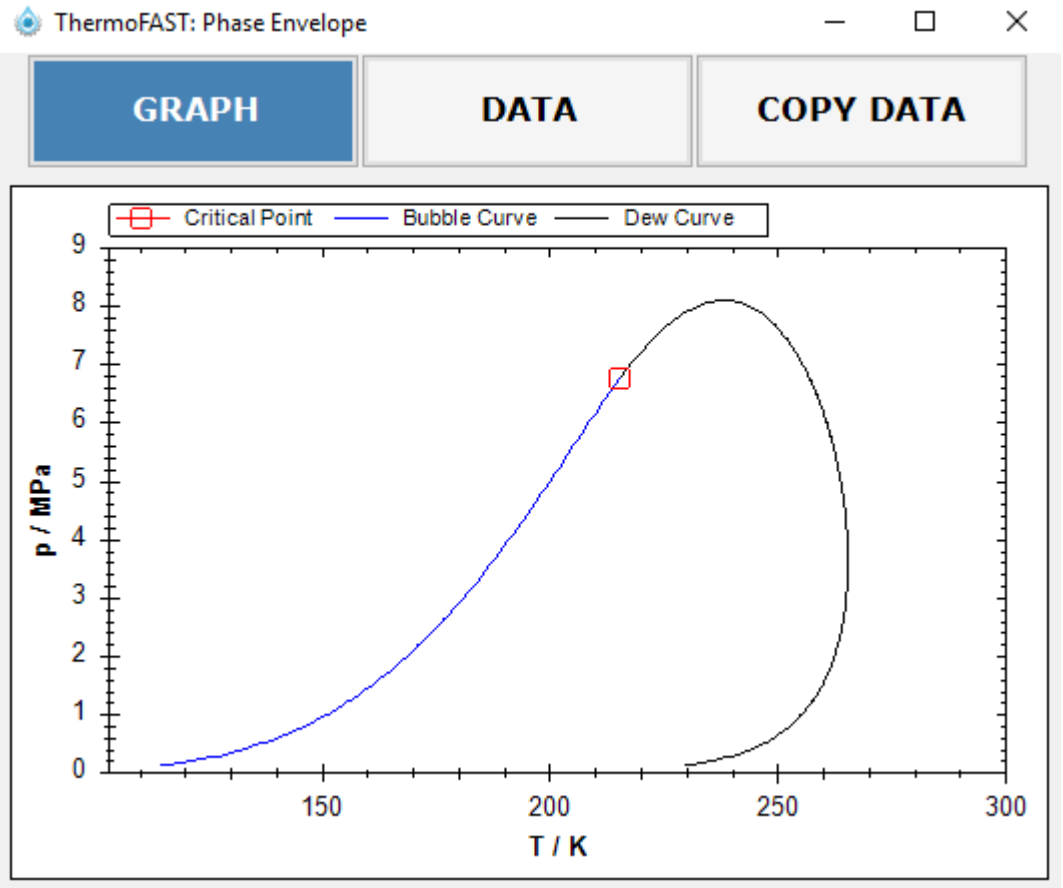

Figure 2.3: Vapour-liquid phase envelope output as generated by ThermoFAST-GPA for the mixture composition given by Figure 2.2.

2.3 FLASH

The FLASH tab (Figure 2.4) allows the user to perform flash calculations at a given temperature and pressure with the outputs being the vapour, liquid and solid phase fractions and densities. In addition, the user is able to perform bubble and dew point calculations at a given temperature or pressure for vapour-liquid conditions, as shown in Figure 2.5. The program will warn the user if solids are possible at the specified VLE conditions.

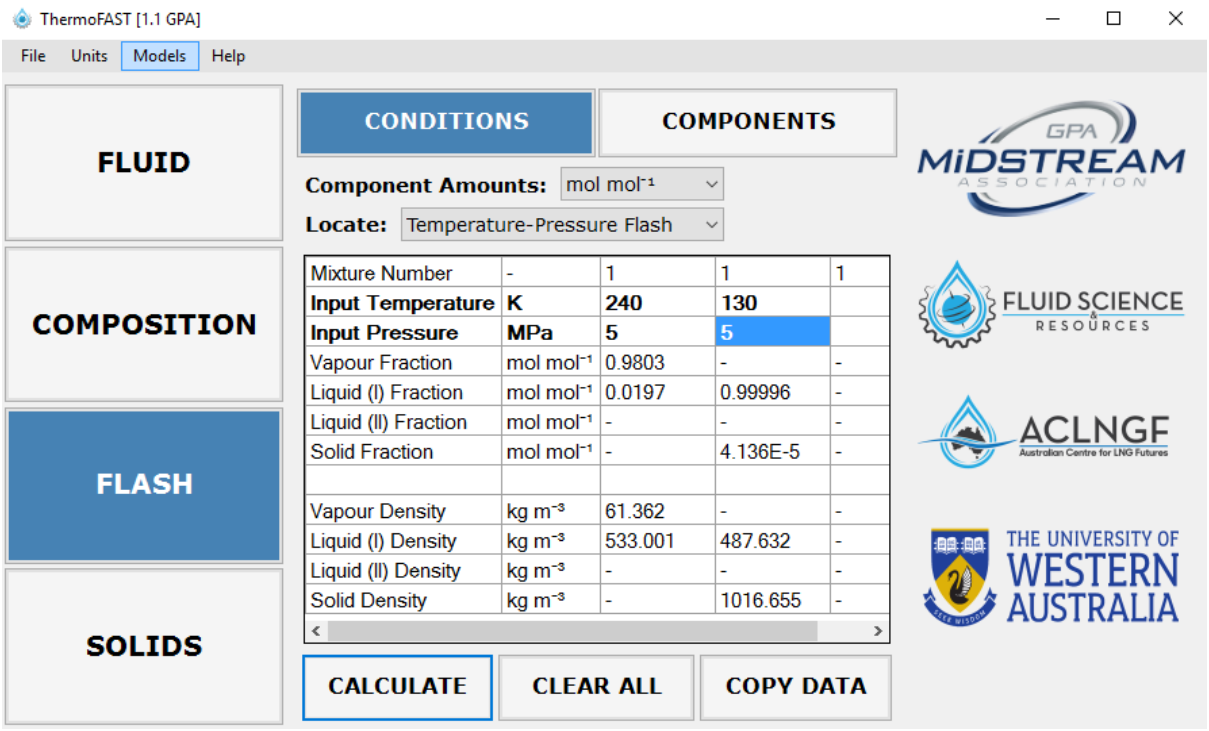

Figure 2.4: ThermoFAST-GPA user-interface showing the "FLASH" tab with example Temperature-Pressure Flash calculations for the mixture composition given by Figure 2.2.

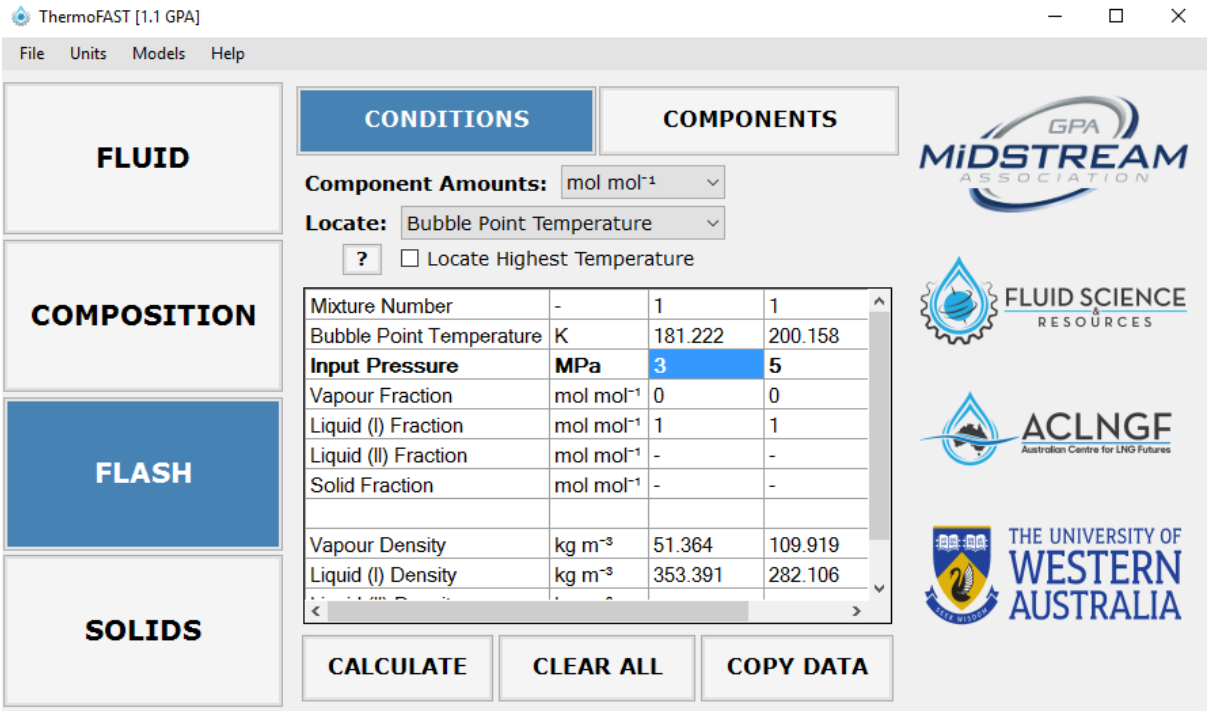

Figure 2.5: ThermoFAST-GPA user-interface showing the "FLASH" tab with example Bubble Point Temperature calculations for the mixture composition given by Figure 2.2.

2.4 SOLIDS

The SOLIDS tab allows users to locate the mixture's highest solid equilibrium temperature (HSET), along with other transitions that occur at temperatures lower than HSET (e.g. SVE to SLE and others described in Section 5). The two major functions in this tab are (1) SEARCH, and (2) GRAPH. The SEARCH function has the following modes of operation:

- TEMPERATURE – locates the solid formation temperature at a given pressure (Figure 2.6), and
- CONCENTRATION – locates the highest allowable concentration of a selected component at a given temperature and pressure (Figure 2.7).

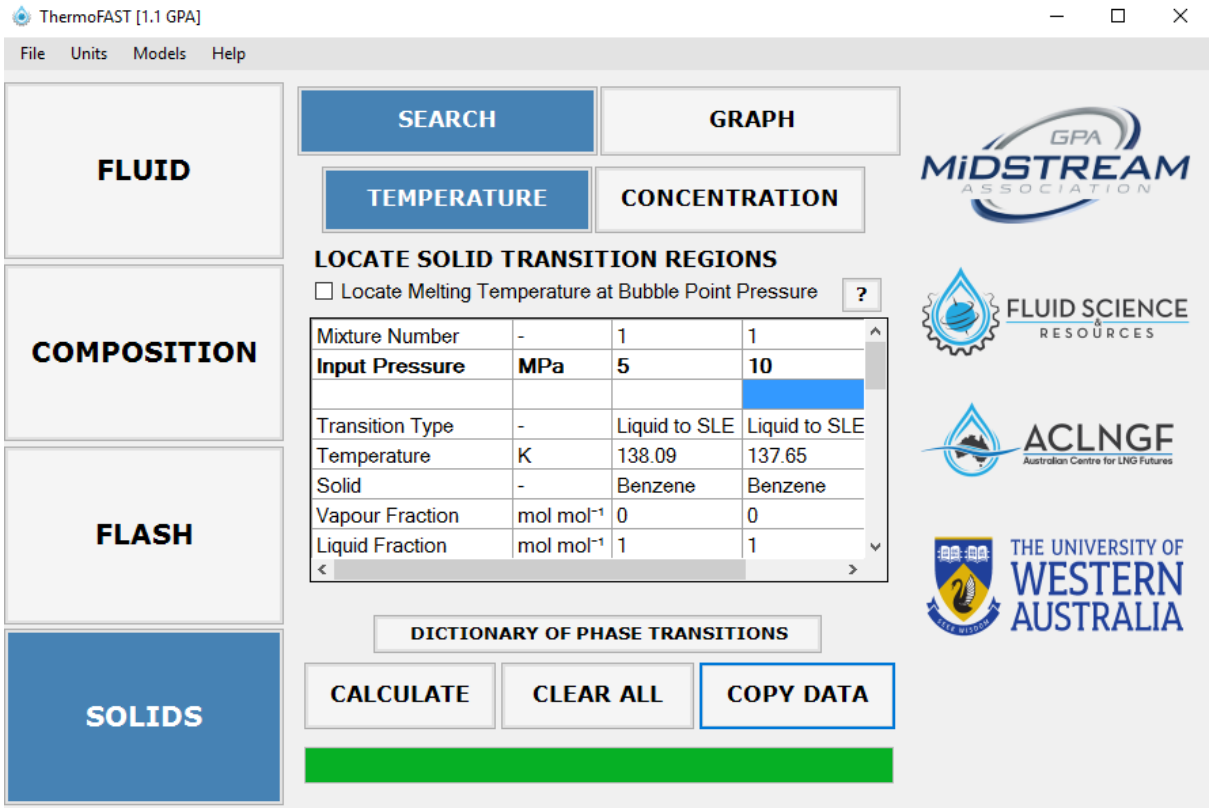

Figure 2.6: ThermoFAST-GPA user-interface showing the "SOLIDS" tab with examples of the SEARCH-TEMPERATURE function for the mixture composition given by Figure 2.2.

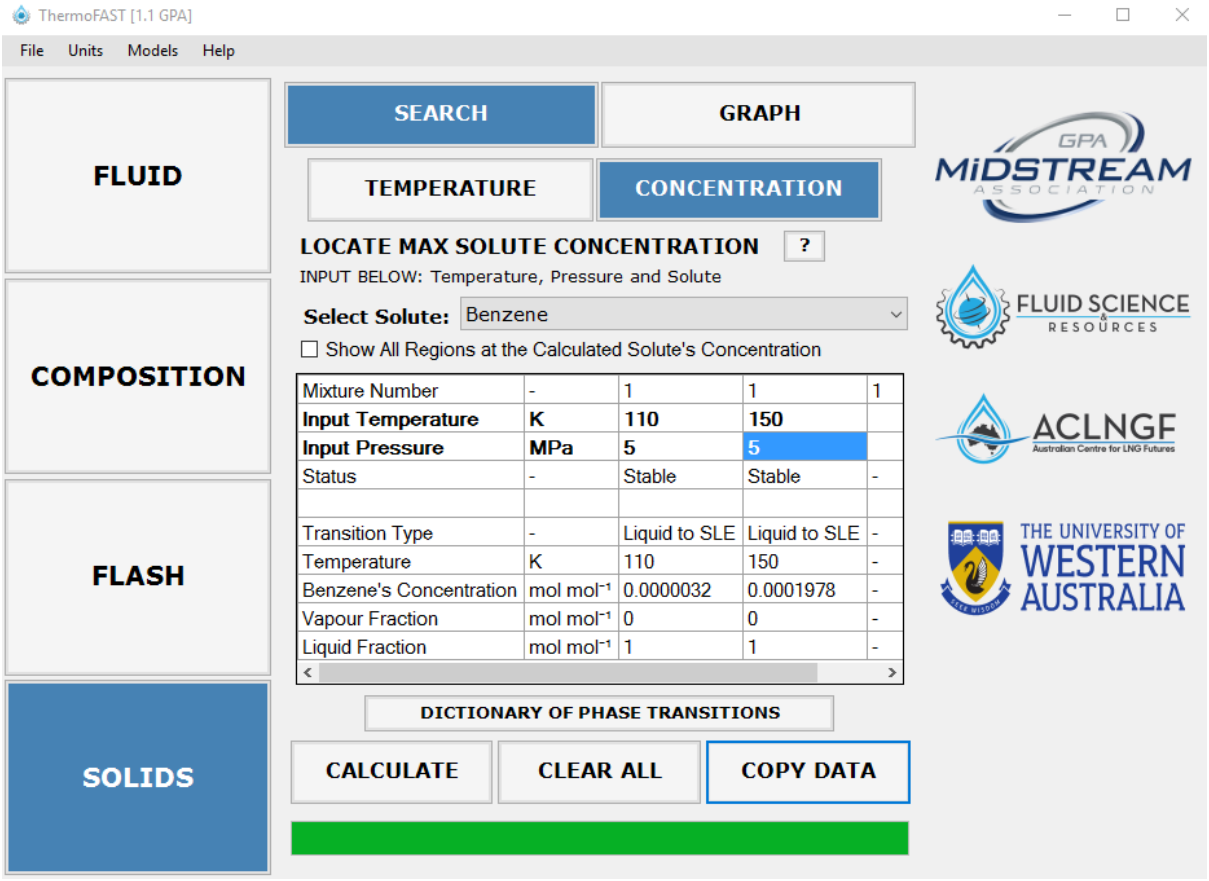

Figure 2.7: ThermoFAST-GPA user-interface showing the "SOLIDS" tab with examples of the SEARCH-CONCENTRATION function for the mixture composition given by Figure 2.2.

The GRAPH function gives the user the option to generate a:

- SOLUBILITY curve – locates HSET with respect to the selected component's concentration at a given pressure,
- SOLID PHASE diagram – locates HSET and other transition temperatures that occur lower than HSET for a fixed mixture composition over a range of pressures, and
- EUTECTIC diagram – locates the Eutectic temperature and HSET with respect to the concentration of the selected component (Figure 2.8).

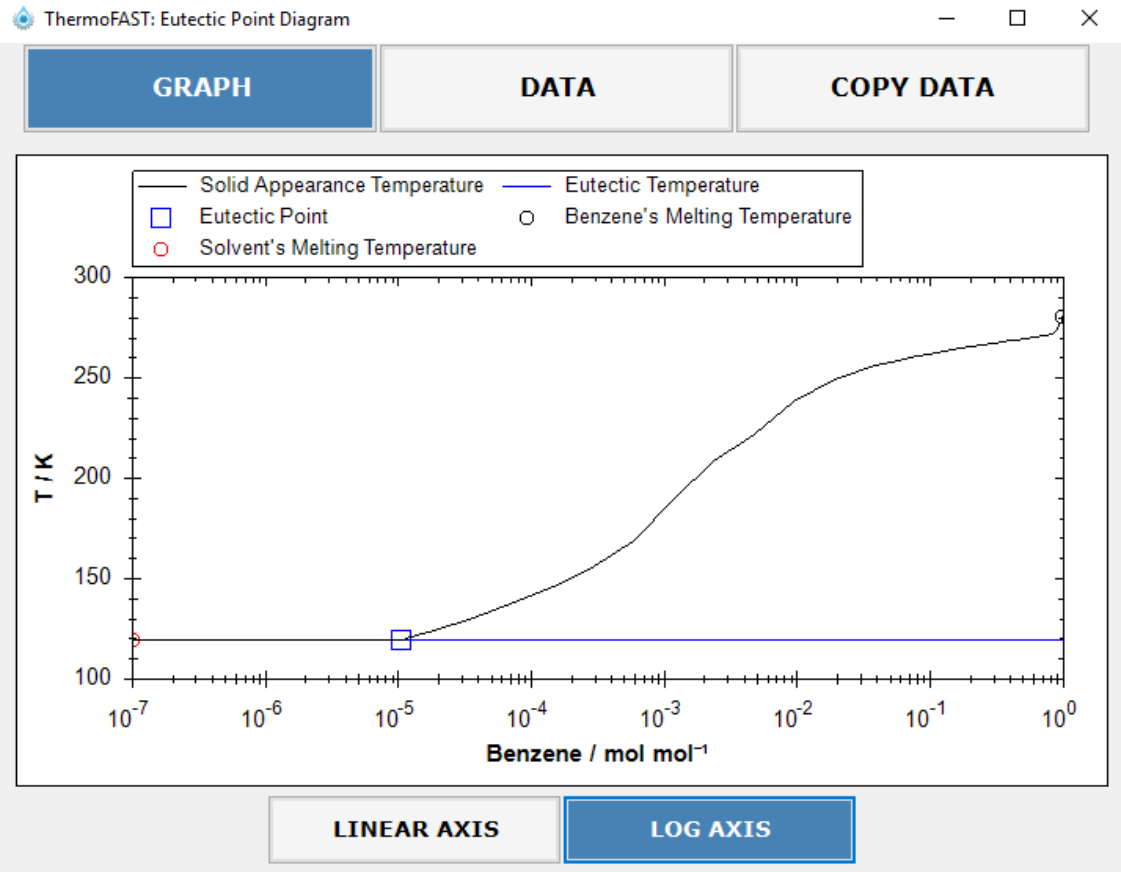

Figure 2.8: Eutectic diagram for the highest solid equilibrium temperature generated by ThermoFAST-GPA showing temperature, T, versus the molar concentration of benzene on a log-scale axis for the mixture composition given by Figure 2.2. The reason for the changes in slope is the presence of vapour-solid and vapour-liquid-solid transitions which occur at higher concentrations of benzene.

3 New Approach for Rapidly Solving Solid-Liquid-Vapour Equilibrium

Central to the calculation of the conditions under which solids form in fluid mixtures is the solution of the phase equilibrium problem. The general solution to such problems where a variable number of phases coexist in a closed system at equilibrium, is determined by following three criteria which must be satisfied for each phase presents (labelled by *k* and *r*)

1. temperature in all phases is equal: $T_r = T_k$ (3.1)
2. pressure in all phases is equal: $P_r = P_k$ (3.2)
3. fugacity of each component in all phases is equal: $f_{i,r} = f_{i,k}$ (3.3)

where, $k = 1\ to\ \pi\ (k \neq r)$,

$\pi =$ number of phases,

$i = 1\ to\ N$, and

$N =$ number of components.

For simple systems or calculations where the number and types of the phases that are present at equilibrium are known or specified beforehand (e.g. vapour and liquid), conditions (1) to (3) can be solved rapidly without difficulty. On the other hand, if the number and types of phases present at equilibrium are not known prior to calculation, a fourth criterion – minimise the Gibbs Energy – can be introduced as was done by Gupta et al. (1991) [19] and Ballard et al. (2004) [20]. However, a disadvantage of this method is that good initial estimates of the unknowns (the amounts and compositions of each phase) are required.

Here a new method is described for solving the general temperature-pressure flash calculation, which does not require such stringent initial estimates of every phase's properties. The method, which is implemented within ThermoFAST utilises a Newton-Raphson based approach similar to those developed by Gupta et al. (1991) [19] and Ballard et al. (2004) [20]; however it requires only initial estimates of how the components partition across any vapour and liquid phases present, which can be done with well-established correlations. This also facilitates the addition of new components into such calculations without the need to develop new correlations for estimating how they partition across all phases that might be present.

3.1 Calculating Component Fugacities in Fluid and Solid Phases

For a flash calculation at a specified temperature and pressure, criteria (1) and (2) are automatically satisfied and therefore the task becomes to find the solution to the fugacity criterion. ThermoFAST utilises the Peng-Robinson cubic equation of state (PR-EOS) [21] to calculate the thermodynamic properties of multi-component fluid mixtures, including vapour-liquid phase equilibrium, at a specified temperature, T, pressure P and overall mole fraction composition, z_i. The PR EOS is utilised due to its structural simplicity and ability to predict VLE behaviour in multi-component hydrocarbon systems without the need for excessive tuning. The (partial) fugacity of a component in a fluid phase of a mixture can be calculated using the PR EOS via the following relationships,

$$ln\left(\frac{f_i}{x_i P}\right) = \frac{B_i}{B}(Z-1) - ln(Z-B) + \frac{A}{2\sqrt{2}B}\left[\frac{B_i}{B} - \frac{2}{a\alpha}\sum_{j=1}^{N} x_j\left(1-k_{ij}\right)\sqrt{a_i a_j \alpha_i \alpha_j}\right] ln\left(\frac{Z+\left(\sqrt{2}+1\right)B}{Z-\left(\sqrt{2}-1\right)B}\right) \quad (3.4)$$

$$a\alpha = \sum_i \sum_j x_i x_j \left(1-k_{ij}\right)\sqrt{(a_i\alpha_i)\left(a_j\alpha_j\right)} \quad (3.5)$$

$$b = \sum_i x_i b_i \quad (3.6)$$

where, $A = \frac{aP}{R^2T^2}$; $B = \frac{bP}{RT}$; $B_i = 0.0778\frac{P_{r,i}}{T_{r,i}}$; $Z = \frac{Pv}{RT}$; α is the PR vapour pressure function (which depends on the reduced temperature and acentric factor [21]); and v is the molar volume of the mixture (also calculated using the PR EOS). Terms with a subscript 'i' refer to the value for a specific component in the mixture: e.g. a_i and b_i are component specific cubic EOS parameters (i.e. for the pure fluid), with $B_i = \frac{b_i P}{RT}$. The binary interaction parameter, k_{ij}, found in eq. (3.4) and (3.5) is usually adjusted to ensure the EOS predicts correctly experimental VLE data for binary mixtures; however it can also be adjusted to force the EOS to correctly predict experimental binary mixture data where a solid phase exists at equilibrium. ThermoFAST uses two sets of binary interaction parameters, one optimised for VLE calculations and another optimised for the prediction of solid equilibrium conditions, as discussed below.

To determine the solubility of a component in a fluid mixture, the partial fugacity of that component calculated using eq (3.4) must be compared with the fugacity of that component in the solid phase. ThermoFAST assumes that any solid phase present consists of a pure substance although multiple (pure) solid phases can be present simultaneously. The fugacity of pure component *i* in the solid phase, f_i^S, is calculated using an equation first derived by Hildebrand and Scott [22] and endorsed by Prausnitz [23],

$$\ln(f_i^s) = \ln\left(\varphi_{pure,i}^L P\right) - \frac{\Delta H_{f,i}}{RT_{m,i}}\left[\frac{T_{m,i}}{T} - 1\right] + \frac{\Delta c_{p,i}^{L\to S}}{R}\left[\frac{T_{m,i}}{T} - 1 + \ln\left(\frac{T}{T_{m,i}}\right)\right] - \frac{\Delta v_i^{L\to S}(P - P_m)}{RT} \tag{3.7}$$

Here, $\varphi_{pure,i}^L$ is the fugacity coefficient of pure component *i* in the liquid phase, (also calculated using the PR EOS); $T_{m,i}$ is the melting temperature of pure component *i*; $\Delta H_{f,i}$ is the corresponding molar heat of fusion at $T_{m,i}$; $\Delta c_{p,i}^{L\to S}$ is the molar specific heat of the component as a pure liquid minus that of the pure solid *i*, which is approximated as being independent of temperature; $\Delta v_i^{L\to S}$ is the change in volume between the liquid and solid phase of component *i*; and P_m is a reference pressure for the given melting temperature, which in this case is atmospheric pressure. Each term on the right of eq (3.7) is calculable from knowledge of the pure component properties, which were taken from various sources including the DIPPR® database [24-27].

3.2 System of Equations for Flash Calculations

The following set of equations describes the material balance for a system of N components distributed across π possible phases

$$\sum_{k=1}^{\pi} \alpha_k x_{ik} = z_i, \qquad i = 1, \ldots, N, \tag{3.8}$$

where, α_k is the normalised phase fraction of phase k and x_{ik} is the mole fraction of component *i* in phase *k*. Particularly when more than three phases are present, it is efficient to specify a reference phase, which must contain all of the components (even in trace concentrations) at equilibrium: accordingly the reference phase should be a fluid, and ThermoFAST selects the liquid phase by default unless the results of an initial VLE(-only) flash indicate that only a vapour phase is present. By considering the reference phase, *r*, eq. (3.8) can be re-written as

$$\alpha_r x_{ir} + \sum_{\substack{k=1 \\ k \neq r}}^{\pi} \alpha_k x_{ik} = z_i, \qquad i = 1, \ldots, N. \tag{3.9}$$

For a closed system, material balance imposes two further constraints on the phase fractions and component mole fractions, respectively,

$$\alpha_r = 1 - \sum_{\substack{k=1 \\ k \neq r}}^{\pi} \alpha_k \,, \qquad k = 1, \ldots, \pi, \tag{3.10}$$

$$\sum_{\substack{k=1 \\ k \neq r}}^{\pi} x_{ik} = 1, \qquad k = 1, \ldots, \pi. \tag{3.11}$$

The requirement that each component's partial fugacity in each phase be equal at equilibrium means that,

$$\frac{f_{ir}}{f_{ik}} = \frac{x_{ir}\phi_{ir}P}{x_{ik}\phi_{ik}P} = 1, \qquad i = 1, \ldots, N, \qquad k = 1, \ldots, \pi \tag{3.12}$$

where f_{ik} and ϕ_{ik} are the partial fugacity and partial fugacity coefficient of component, *i*, in phase, *k*, respectively. This representation of the third criterion, eq. (3.3), allows the problem to be conveniently recast in terms of calculating the equilibrium (or partition) coefficients, $K_{ik} \equiv x_{ik}/x_{ir}$ for component *i* across phases *k* and *r*. With initial estimates of x_{ir} and K_{ik}, the compositions of other phases present can be estimated by solving the material balance equations (3.7) to (3.9). New estimates of the equilibrium coefficients can then be generated using equations (3.4) and (3.5) for any fluid and solid phases present, respectively, via:

$$K_{ik} = \frac{\phi_{ir}}{\phi_{ik}} = \frac{x_{ik}}{x_{ir}} \frac{f_{ir}}{f_{ik}}, \qquad i = 1, \ldots, N, \qquad k = 1, \ldots, \pi \tag{3.13}$$

An iterative procedure is then followed until the calculated phase compositions and fractions converge within a specified tolerance. The remaining key steps, then, are achieving sufficiently good initial estimates of K_{ik} and establishing which phases are stable and hence present at equilibrium.

3.3 Solving the Flash Calculation

Figure 3.1 shows the logical flow of the primary algorithm used by ThermoFAST to solve the majority of flash calculations. The algorithm works by performing an initial VLE-only flash, using well-established correlations [28] to provide initial estimates for the K_{ik} of the fluid

phases. Since all solid phases are pure compounds and the composition of the reference phase has been estimated using the initial VLE-only flash, calculation of the solid phase fugacity using eq (3.7) for each component at the specified temperature and pressure provides an initial estimate of the K_{ik} for the solid phase(s). These then allow a solid-liquid equilibrium flash calculation to provide an estimate of the phase fractions α_k: stable phases have $\alpha_k > 0$.

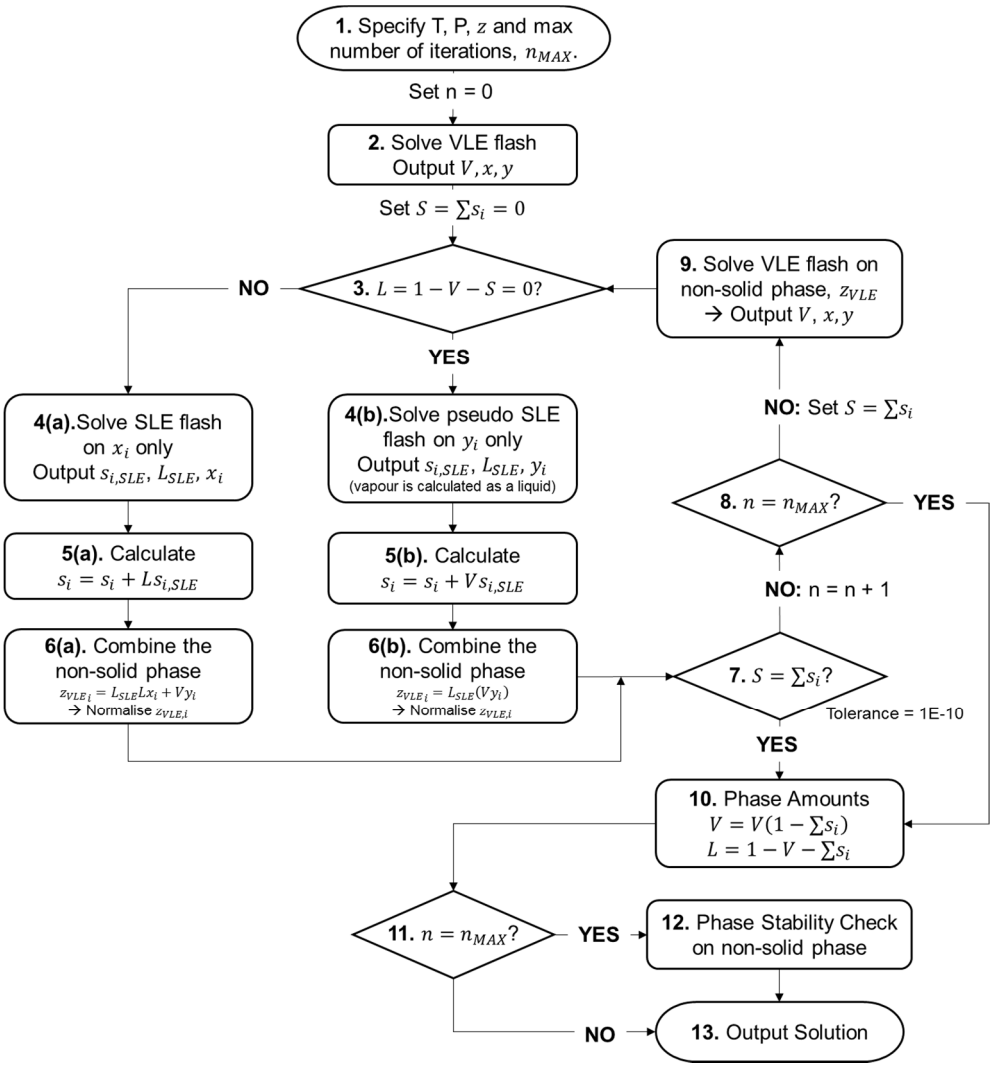

Figure 3.1: ThermoFAST's isothermal algorithm for solving vapour-liquid-solid equilibrium using a successive substitution method. The VLE and SLE flash algorithms are given in Baker et al. (2018) [3] and Baker (2018) [29] . Here, *T* is temperature, *P* is pressure, *z* is overall composition, *i* represents a particular single component, *f* is fugacity, *s* is the solid composition, *x* is liquid composition, *y* is vapour composition, φ^L is the partial fugacity in the liquid phase, *V* is the overall vapour mole fraction, *L* is the overall liquid mole fraction, n is the number of iterations, n_{max} is the maximum number of iterations, and the subscript SLE refers to any variable determined from the SLE Flash algorithm within the multiphase equilibrium calculation as described in Baker et al. (2018) [3]. The phase stability check is performed by calculating the bubble point, T_{bub}^{VLE}, on the non-solid phase and if $T_{bub}^{VLE} < T$ then $V = 0$ and $L = L + V$, otherwise $V > 0$ (and if vapour did not exist then $V = L$ and $L = 0$).

This procedure is iterated until either convergence is achieved in the x_{ik} and α_k, or the specified maximum number of iterations is reached. Often the tolerance criterion is achieved within three iterations and the maximum number of iterations is set to five. If this condition is reached then the outputs of the (unconverged) calculation are used as improved initial estimates within a more complicated numerical algorithm based on the work of Gupta et al. (1991) [19] and Ballard et al. (2004) [20] and incorporates a Newton-Raphson algorithm to achieve a rapid convergence, rather than the slower (but less sensitive) successive substitution method used for the algorithm shown in Figure 3.1. Further detail about this algorithm and its implementation in ThermoFAST is given in Baker (2018) [29].

4 Comparison with Experimental Data

ThermoFAST has been tuned to solid-fluid equilibrium data for 60 binary systems relevant to LNG and natural gas production. The binary interaction parameters k_{ij} in eq. (3.4) were adjusted using the Levenberg-Marquardt non-linear least squares regression method to minimise the following objective function,

$$ObjFunc = \sum_{i=1}^{N} \left(T_{i,meas} - T_{i,calc}\right)^2 \tag{4.1}$$

Here, i is an index over the N data points available for a given binary mixture, $T_{i,meas}$ is the measured solid equilibrium temperature, and $T_{i,calc}$ is the solid equilibrium temperature calculated using ThermoFAST. The binary systems considered consisted of pairs of the following compounds: alkanes from methane to n-decane (including isobutane, isopentane, and neo-pentane), CO_2, cyclopentane, cyclohexane, methyl-cyclohexane, and the aromatics benzene, toluene, ethylbenzene, m-xylene, o-xylene, and p-xylene. Of the possible binary pairs from this list of compounds, only 60 systems had sufficient quality data to reliably tune a k_{ij} optimised for solid equilibrium predictions. For solid equilibrium calculations involving any of the remaining pairs, ThermoFAST uses binary interaction parameters optimised for VLE predictions.

Table 4.1 shows a summary of the performance of the tuned ThermoFAST and KLSSP models in representing the available experimental data. Three different scenarios were used to quantify the performance of each model: (1) all 60 binary mixtures over the entire experimental range, (2) the binary mixtures that contain components available within KLSSP and (3) binaries that

are available and within KLSSP's range of validity as per Table 1.1. The standard user interface available for KLSSP does not allow calculations outside its range of validity; however the Visual Basic interface to KLSSP implemented within Microsoft Excel allows these limits to be bypassed. In addition, a detailed table of the root mean square deviations (rmsd) for each individual binary system applicable to the three scenarios are given in Appendix A via Table 8.1 to Table 8.3 for both ThermoFAST and KLSSP.

Table 4.1: Summary of ThermoFAST and KLSSP predictions for the available literature data for solid equilibria in binary mixtures according to three criteria: (A) all 60 binary systems, (B) 36 binary systems that can be calculated in KLSSP as per Table 1.1 and (C) 17 binary systems that are available in KLSSP and are within KLSSP's recommended range of validity as per Table 1.1. Shown is the average, minimum and maximum of the root-mean-squared temperature deviations (rmsd) between the model and literature data, as well as the standard deviation, σ_x, and the median. For case (A) the performance of an un-tuned ThermoFAST model with k_{ij} = 0 is shown. For each individual binary system applicable to the three scenarios are given in Appendix A via Table 8.1 to Table 8.3 for both ThermoFAST and KLSSP.

CRITERIA	**MODELS**	***rmsd* / *K***			σ_x / *K*	***Median* / *K***
		Avg.	Min.	Max.		
(A) all binary mixtures	***ThermoFAST (Tuned)***	1.7	0.1	7.6	1.8	1.2
	ThermoFAST (k_{ij} = 0)	11.1	0.2	60.6	13.6	4.7
(B) binaries limited to components in *Table 1.1*	***ThermoFAST (Tuned)***	1.6	0.1	7.6	1.6	1.0
	KLSSP	19.1	0.5	64.0	19.1	8.8
(C) binaries and compositions limited to *Table 1.1*	***ThermoFAST (Tuned)***	1.1	0.2	5.2	1.2	0.8
	KLSSP	5.6	0.5	16.4	5.1	3.6

Table 4.1 shows that by tuning the k_{ij} ThermoFAST can represent all of the data for all binaries with an average rmsd of 1.7 K across all binaries. Using KLSSP outside its stated range of validity produces an average rmsd almost twice as large as the un-tuned PR EOS model (k_{ij} = 0), which reflects the general advantage of using an equation of state over an activity coefficient model. Within its range of validity, the average rmsd of the KLSSP model is 4.5 K larger than that of the tuned ThermoFAST model. Thus not only does the ThermoFAST improve upon KLSSP's range of validity in terms of conditions and compounds considered, it also describes more accurately those data that are outside the range of validity. In the following two subsections graphical comparisons are presented for a selection of binary and multi-component mixtures where data relevant to gas processing are available.

4.1 Exemplar Binary Mixtures

Figure 4.1 to Figure 4.5 show the solid equilibrium predictions of ThermoFAST and KLSSP together with the experimental data for the following binary mixtures containing methane or ethane with benzene, p-xylene, cyclohexane, neopentane and CO_2, respectively.

In the methane + benzene system shown Figure 4.1, KLSSP clearly represents the available data well at the low concentrations of benzene that are of relevance to LNG production. It appears to have been tuned to slightly under-predict the equilibrium temperature probably to ensure any error produced was of a conservative nature. ThermoFAST is also able to represent the data well but over the entire range of compositions for which measurements exist. Within its recommended limits, KLSSP represents the data with an rmsd of 8.4 K while ThermoFAST has an rmsd of only 1.5 K.

Figure 4.2 shows data for the system methane + cyclohexane. The KLSSP predictions are generally reasonable although it is unable to represent the pressure dependence of certain data even within its range of validity as shown in Figure 4.2(a). In contrast ThermoFAST is able to capture the large changes in the solid equilibrium temperature that occur with pressure and cyclohexane concentration, improving the rmsd by a factor of 20.

Two binary systems not described by KLSSP containing p-xylene and neopentane are shown in Figure 4.3 and Figure 4.4, respectively. ThermoFAST represents the experimental data for the system methane + p-xylene (Figure 4.3(a)), with an rmsd of only 0.7 K, while for ethane + p-xylene binary (measured over a wider range of conditions) the rmsd is less than 2.7 K. Figure 4.4 shows the results for the methane + neopentane system for which only three data points are available. These solid equilibrium data were measured along the system's bubble-point curve; the ThermoFAST user interface (Figure 2.6) allows the user to specify solid equilibrium temperatures should be calculated according to this constraint. The tuned ThermoFAST model does not represent dependence of melting temperature with neopentane concentration, as well as it does for most tuned binary systems. This result provides further motivation to acquire additional solid equilibrium data for methane + neopentane binary.

Figure 4.5 shows ThermoFAST is able to represent the experimental data available for the methane + CO_2 binary system very well across the complete range of CO_2 fraction. The largest deviations to experimental data for both ThermoFAST and KLSSP is that of Pikaar (1959)

[30], where deviations of (14 and 23) K were observed to ThermoFAST and KLSSP, respectively. This data set, although shown in Figure 4.5, has been excluded from tuning as it showed repeat measurements to deviate up to 27 K at the lowest concentrations of CO_2. At these low CO_2 concentrations relevant to LNG production and within KLSSP's range of validity, the tuned ThermoFAST model has an rmsd of only 2.2 K, compared with 16.4 K for the KLSSP model. Including the 41 additional conditions extracted from Pikaar (1959), the overall rmsd at the same conditions are (3.0 and 16.2) K for ThermoFAST and KLSSP, respectively.

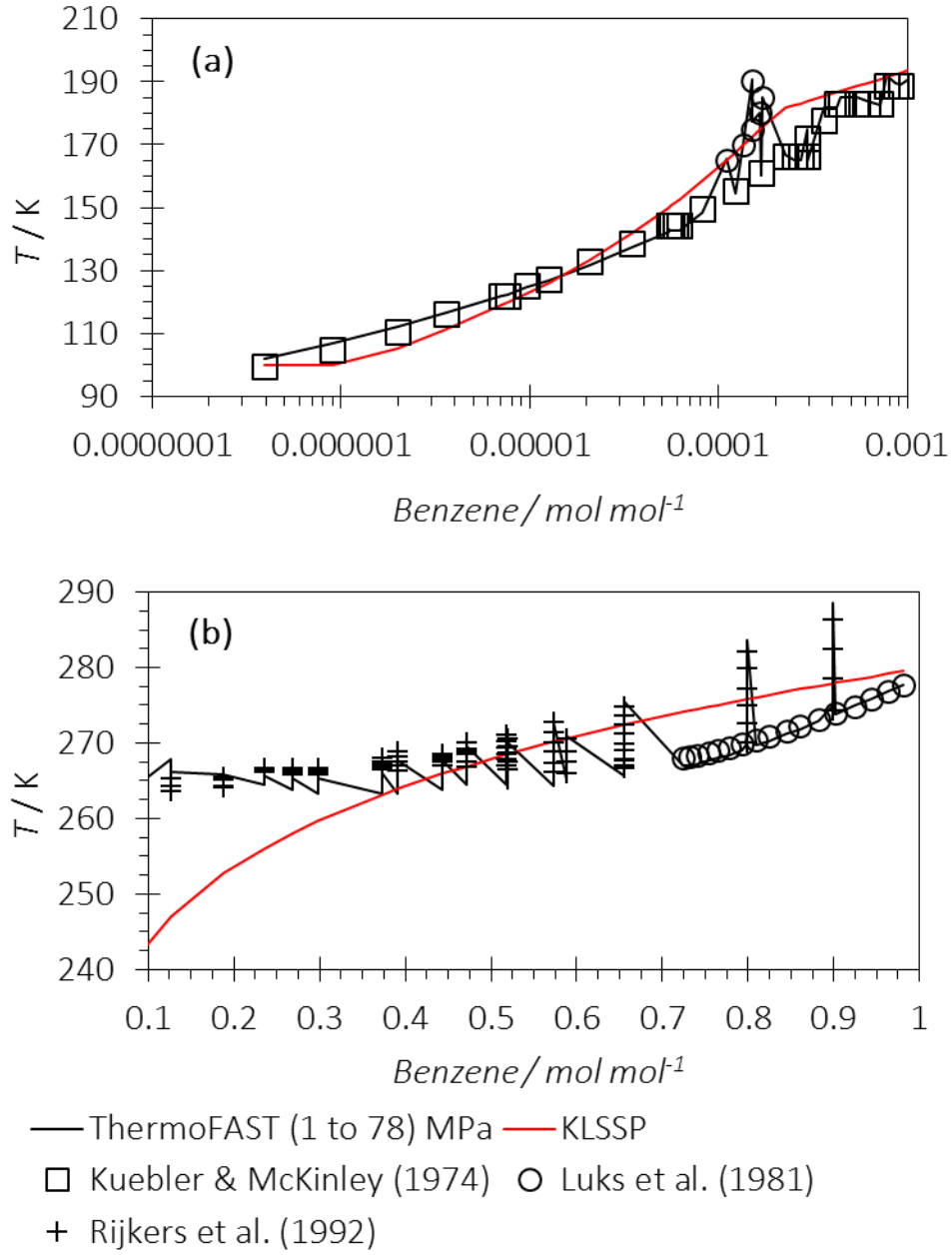

Figure 4.1: Solid-equilibrium diagram for methane + benzene comparing ThermoFAST and KLSSP solid equilibrium predictions against experimental data [14, 31, 32] at (a) low and (b) high concentrations of benzene. ThermoFAST uses the experimental pressure as an input together with the composition.

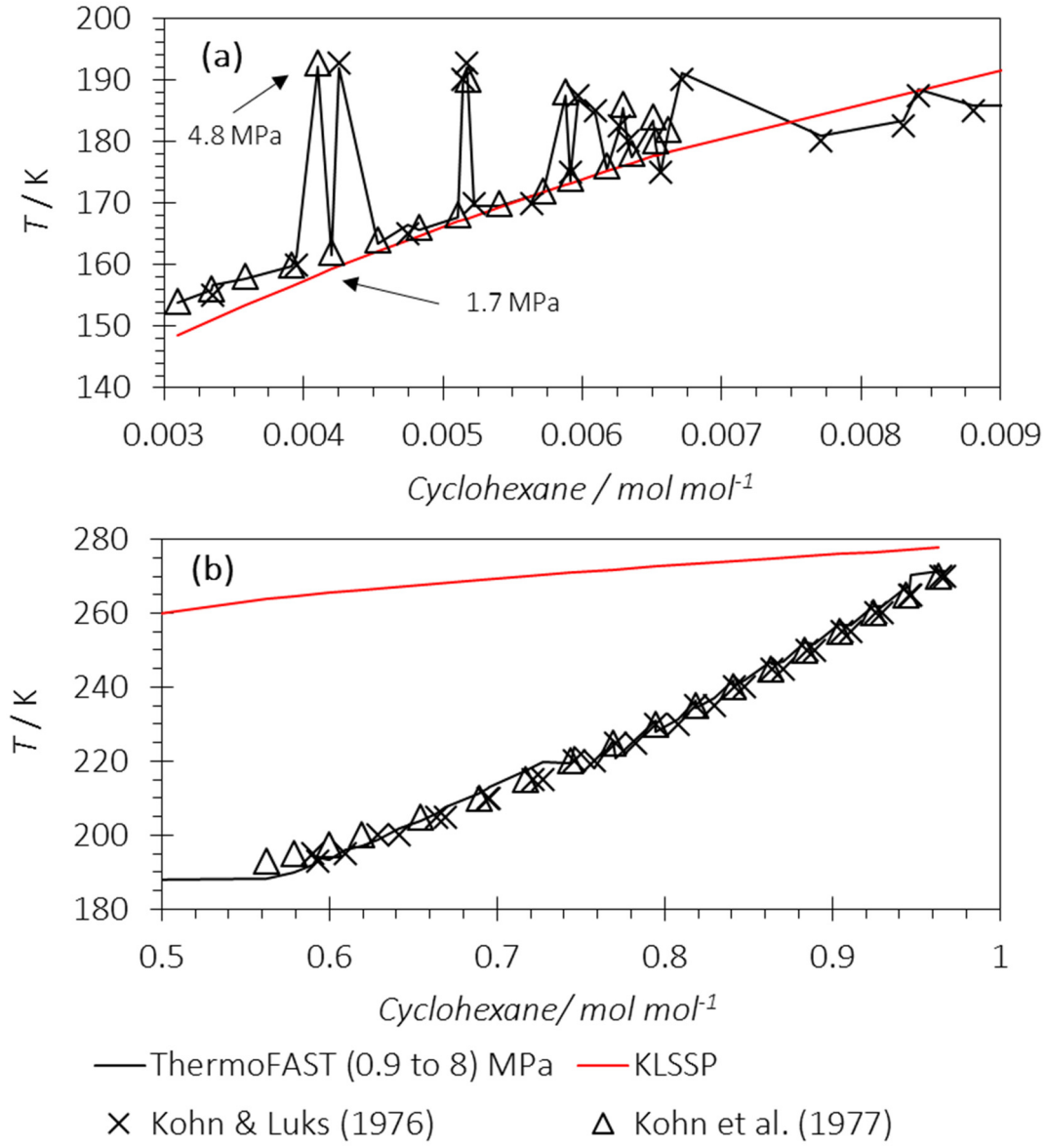

Figure 4.2: Solid-equilibrium diagram for methane + cyclohexane comparing ThermoFAST and KLSSP solid equilibrium predictions against experimental data [5, 17] at (a) low and (b) high concentrations of cyclohexane. ThermoFAST uses the experimental pressure as an input together with the composition.

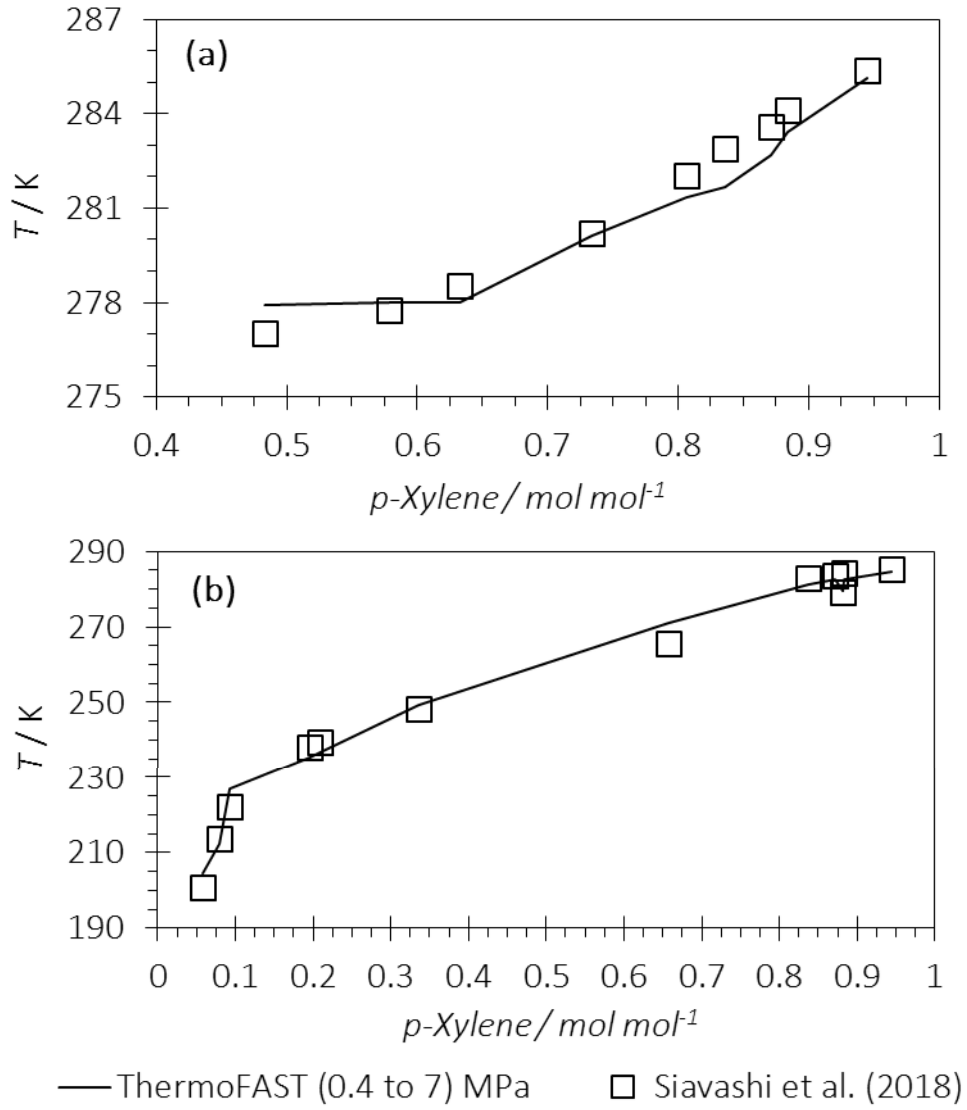

Figure 4.3: Solid-equilibrium diagram for (a) methane + p-xylene and (b) ethane + p-xylene comparing ThermoFAST predictions against experimental data [33]. ThermoFAST uses the experimental pressure as an input together with the composition.

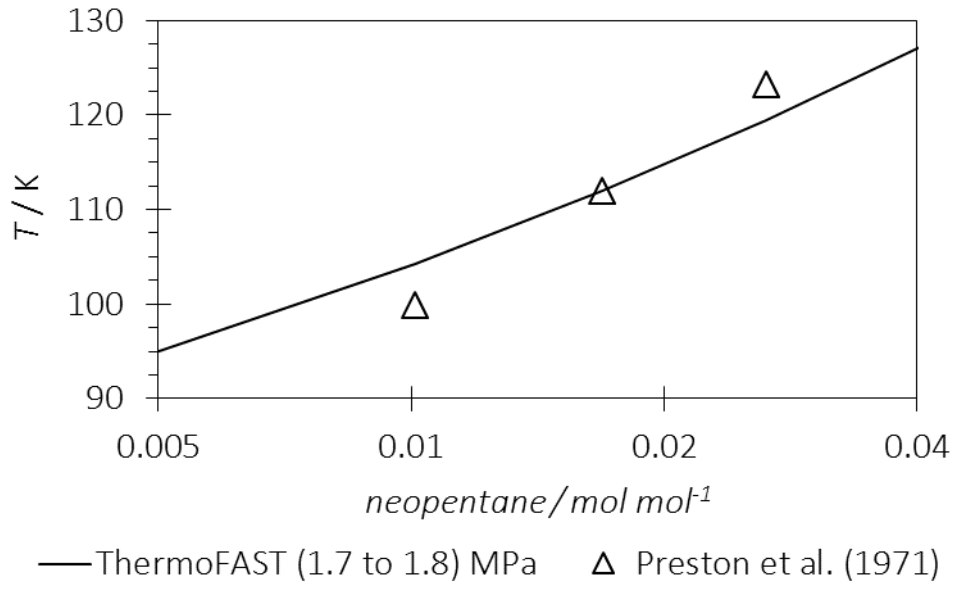

Figure 4.4: Solid-equilibrium diagram for methane + neopentane comparing ThermoFAST predictions against the limited available data [34], which were measured along the bubble point curve..

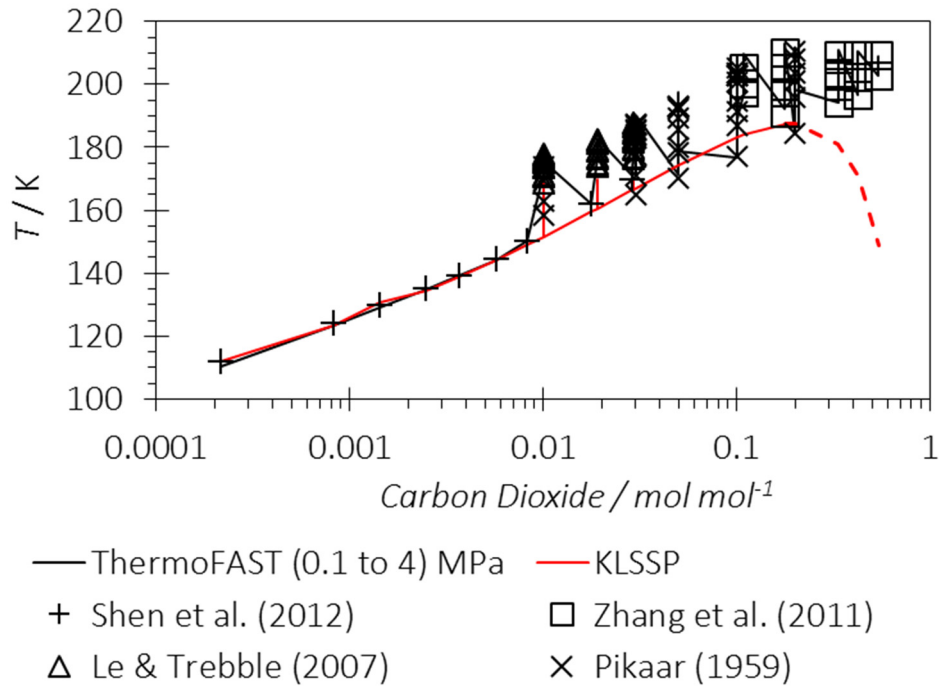

Figure 4.5: Solid-equilibrium diagram for methane + carbon dioxide (CO_2) comparing ThermoFAST and KLSSP solid equilibrium predictions against experimental data [30, 35-37]. ThermoFAST uses the experimental pressure as an input together with the composition. The dashed lined section of KLSSP shows where the model has not been fitted (KLSSP's stated range of validity for CO_2 < 0.15 mol mol^{-1}).

4.2 Exemplar Multicomponent Mixtures

Table 4.2 summarises the comparisons of ThermoFAST and KLSSP predictions with data available for five multicomponent (MC) mixtures containing hexane, heptane, octane, benzene

and cyclohexane. The ThermoFAST predictions have an rmsd of less than 3 K from the experimental data for each multicomponent system except those containing cyclohexane, where the rmsd was 10.6 K. Figure 4.6 to Figure 4.8 show comparisons for some of the MC mixtures containing octane, benzene and cyclohexane solutes, respectively.

Table 4.2: Summary of ThermoFAST and KLSSP predictions for available multicomponent solid equilibrium data. Shown is the average of the root-mean-squared temperature deviations (rmsd) between the model and literature data, as well as the ranges of pressure and methane mole fraction.

	rmsd / K		*p*/ MPa		CH_4 / mol mol^{-1}	
	ThermoFAST	KLSSP	*Max*	*Min*	*Max*	*Min*
$C_1 + C_2 + C_3$ *Solid: nC_6H_{14}*	2.9	8.0	0.9	0.1	0.846	0.346
$N_2 + C_1 + C_2 + C_3 + nC_4$ *Solid: nC_7H_{16}*	1.0	20.7	2.7	0.8	0.949	0.329
$N_2 + C_1 + C_2 + C_3 + iC4 + nC_4 + nC_6 + nC_7$ *Solid: nC_8H_{18}*	1.6	10.0	5.1	0.1	0.966	0.036
$C_1 + C_2 + C_3 + iC4 + nC_4$ *Solid: C_6H_6 (benzene)*	2.1	9.9	16.0	< 0.1	0.891	0.036
$C_1 + C_2 + C_3 + iC4 + nC_4$ *Solid: C_6H_{12} (cyclohexane)*	10.6	16.8	3.8	0.1	0.888	0.040

Figure 4.6 shows comparisons of KLSSP and ThermoFAST predictions to experimental data for a MC mixture with octane as the solute in solvents containing varying concentrations of N_2, CH_4, C_2H_6, C_3H_8, iC_4H_{10}, nC_4H_{10}, nC_6H_{14} and nC_7H_{16} at pressures between (0.1 and 5.1) MPa. ThermoFAST agrees well with the experimental data across the entire composition and pressure range with an overall rmsd of only 1.6 K. For the data sets measured through the GPA research program, KLSSP does a good job at representing solubilities at low to moderate concentrations, even though those data were not used in the model's regression. However, KLSSP deviates by up to 30 K from the low concentration data of Chen et al. (1981) [12], with an overall rmsd of 10.0 K to all data.

Figure 4.7 shows comparisons of KLSSP and ThermoFAST predictions to experimental data for benzene in solvents containing varying concentrations of CH_4, C_2H_6, C_3H_8, iC_4H_{10} and nC_4H_{10} at pressures varying between (0.0 and 16.0) MPa. ThermoFAST has a good agreement across the entire data range with an rmsd of only 2.1 K. In contrast the KLSSP predictions of melting temperature are systematically low across the entire benzene concentration range with an rmsd of 9.9 K. At certain low benzene concentrations, the KLSSP predictions are in good agreement with the data; however deviations as large as 24 K also occur in this region.

Figure 4.8 shows comparisons of KLSSP and ThermoFAST predictions to experimental data for cyclohexane in solvents containing varying concentrations of CH_4, C_2H_6, C_3H_8, iC_4H_{10} and nC_4H_{10} at pressures varying between (0.1 and 3.8) MPa. Both ThermoFAST and KLSSP perform relatively poorly with an rmsd of 10.6 K and 16.8 K, respectively. Two sets of ThermoFAST predictions are shown in Figure 4.8, one in which the pressure was entered as an input, and one where the liquid was instead specified to be at its bubble point.

Though, despite the abundance of individual data points as shown in Figure 4.8(b) it is recommended that new high quality reference data sets be acquired as the stated experimental phases did not exist at the higher concentrations unless the pressure was altered to match the triple point pressure (the point at which the solid appears at the bubble point). This is the method at which these data sets were measured, along the bubble point curve, and the stated low pressure points do not appear reliable especially as their recorded pressures were regularly below atmosphere, also reinforcing the importance of accurate pressure measurements in the calculation of solid equilibrium temperatures.

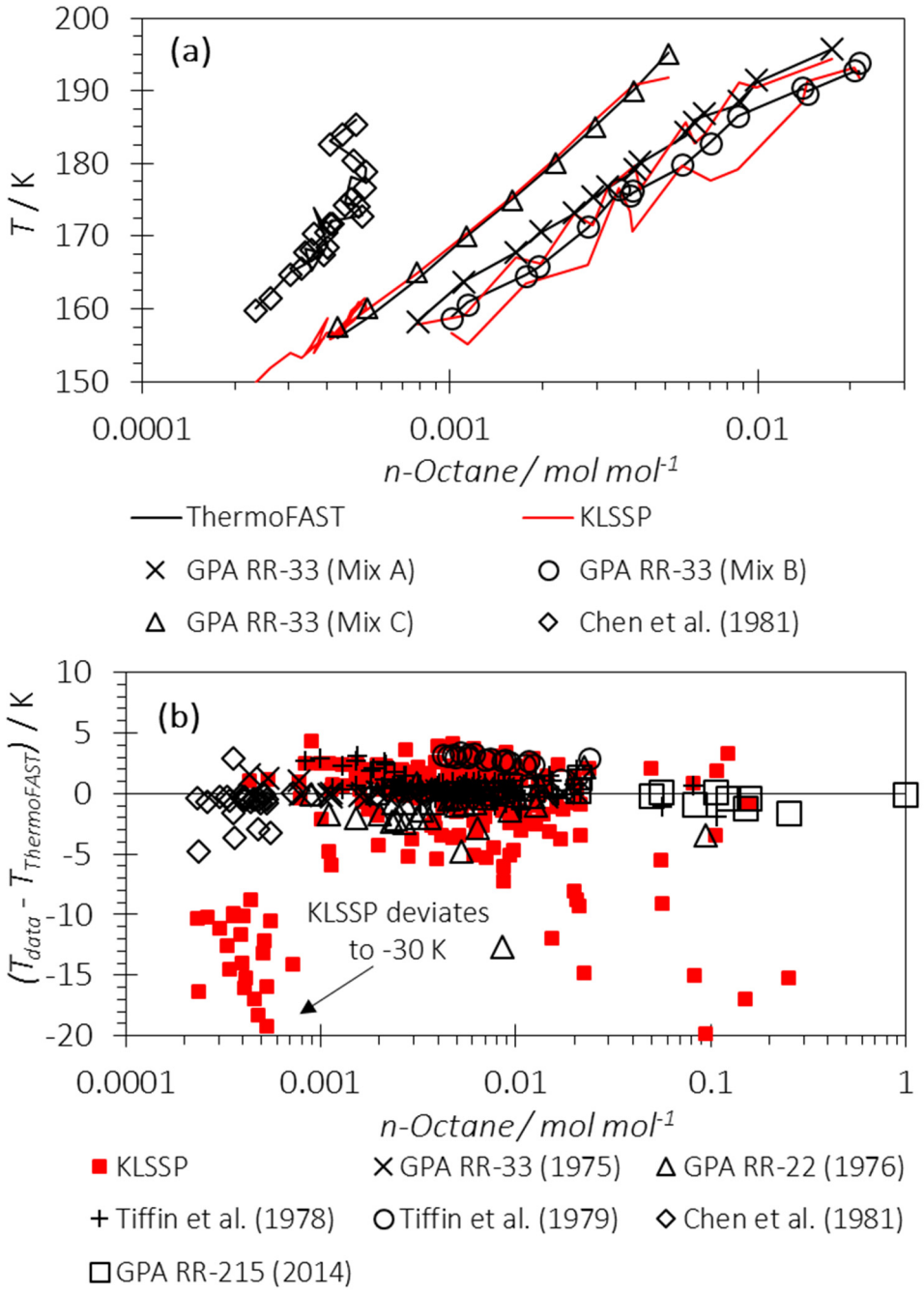

Figure 4.6: (a) Solid equilibrium data for a range of multicomponent systems containing octane as the solute and the corresponding predictions of ThermoFAST and KLSSP. Mix A is a N_2, 0.89 CH_4 to 0.02 nC_4H_{10}; Mix B is a 0.87 CH_4 to 0.02 nC_6H_{14}; Mix C is a 0.94 CH_4 to 0.02 C_3H_8. (b) Deviations of melting temperatures predicted by ThermoFAST and KLSSP from all the experimental data [7, 10, 12, 16-18]. For clarity, only some of the data points represented in (b) are shown in (a).

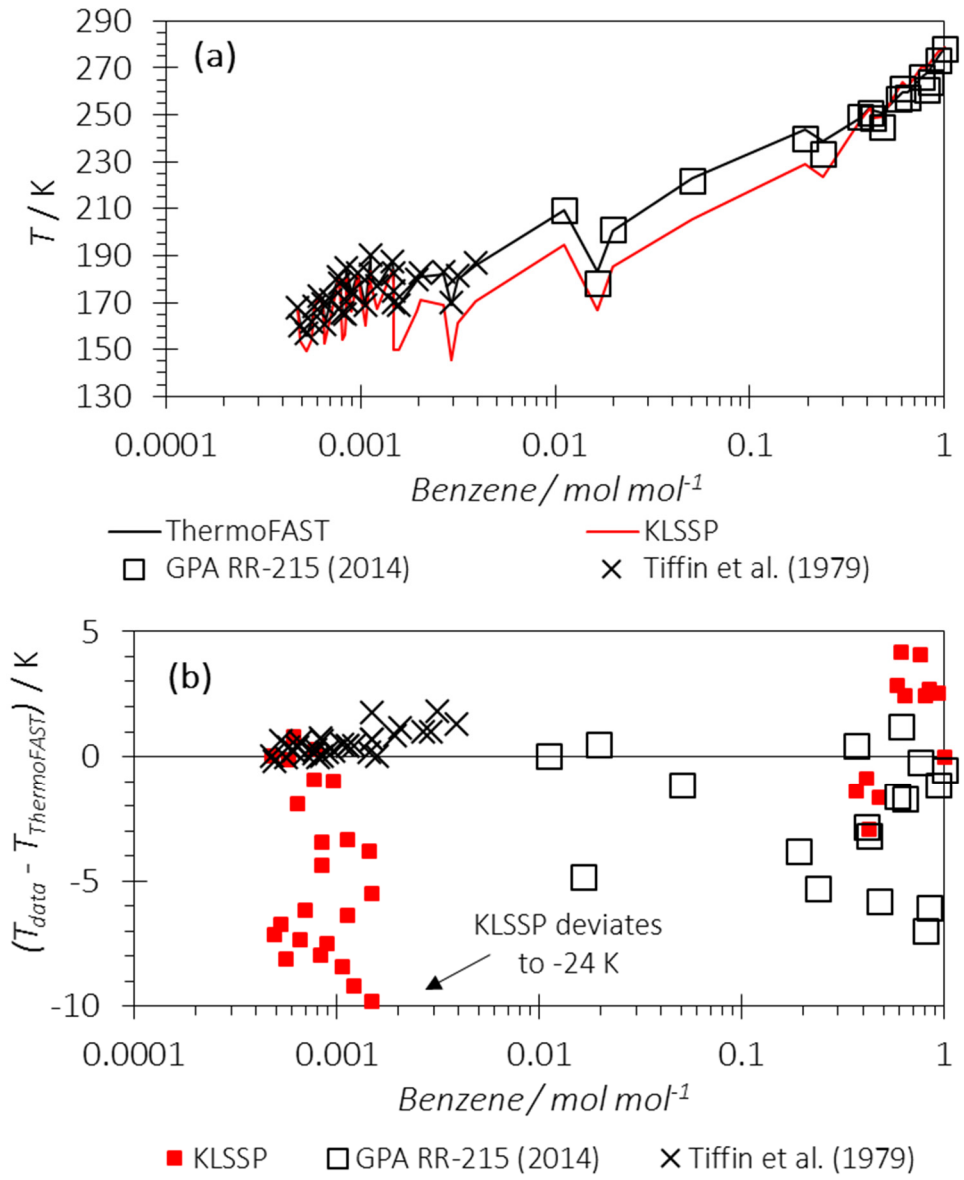

Figure 4.7: (a) Solid equilibrium data for a range of multicomponent systems containing benzene as the solute and the corresponding predictions of ThermoFAST and KLSSP. (b) Deviations of melting temperatures predicted by ThermoFAST and KLSSP from all the experimental data [9, 18]. For clarity, only some of the data points represented in (b) are shown in (a).

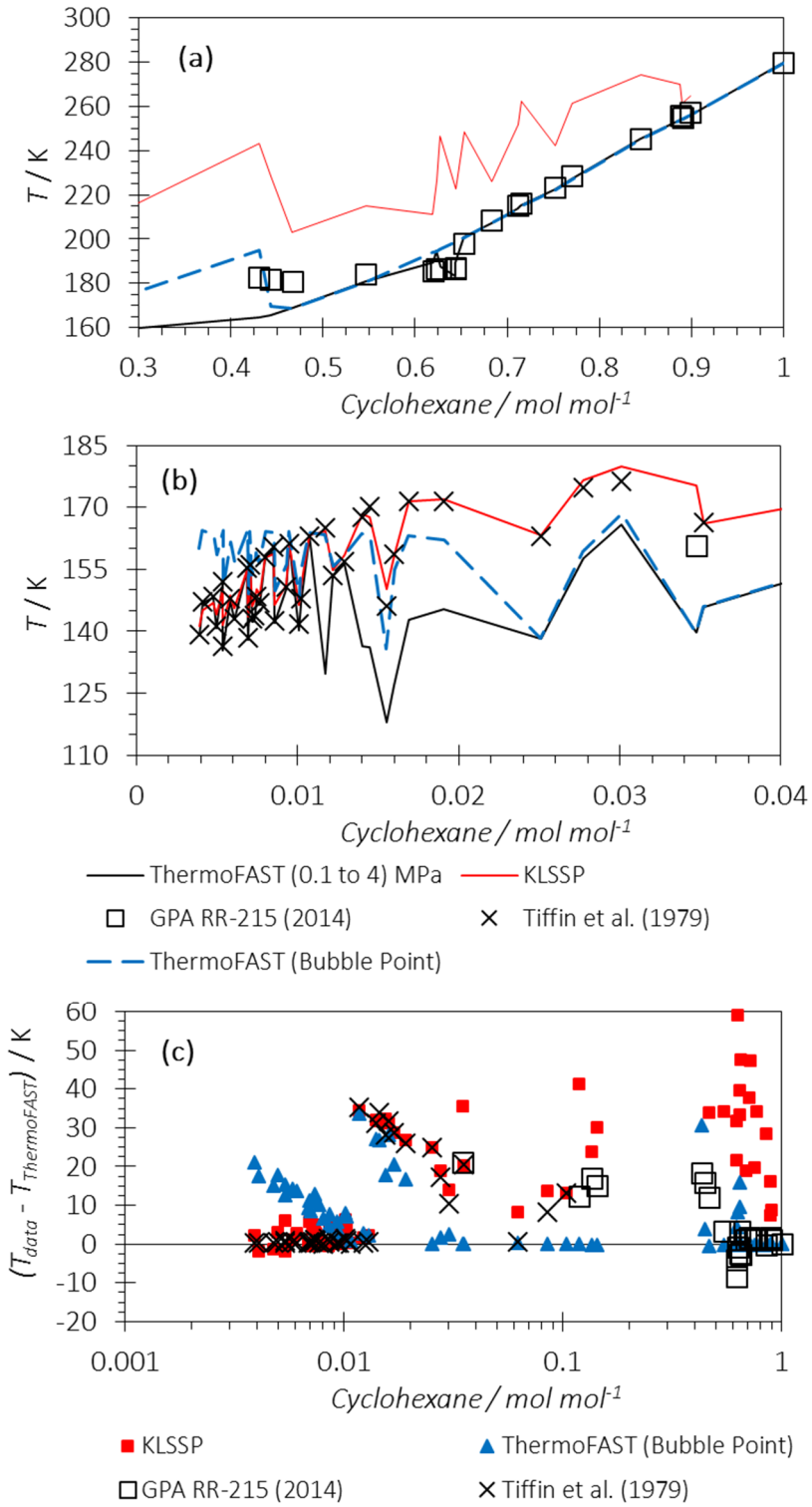

Figure 4.8: Solid equilibrium data for a range of multicomponent systems containing (a) high and (b) low concentrations of cyclohexane as the solute and the corresponding predictions of ThermoFAST and KLSSP. The data points were measured at different solvent compositions and pressures which accounts for the variability in the trends with concentration. The "ThermoFAST (Bubble Point)" values were calculated by specifying the solid equilibrium condition occurred on the bubble point curve, which reflects an experimental method often used for such measurements. (c) Deviations of melting temperatures predicted by ThermoFAST and KLSSP from all the experimental data [9, 18].

5 Solid Phase Transitions in Mixtures

The Peng Robinson EOS together with flash algorithms for calculating phase equilibria over wide ranges of temperature, pressure and composition, allows ThermoFAST to determine the location and nature of multiple transitions involving the appearance or disappearance of solid phases along a given pathway. The solids search algorithm presented in Figure 2.6 allows the user to search along a constant pressure pathway for all the temperatures at which a transition occurs where a solid is or becomes present upon further cooling. Often, there is only one such temperature as shown in Figure 5.1 for pure CO_2, which shows examples of a liquid to solid transition (#1) and a vapour to solid transition (#2). However, in mixtures the extra degrees of freedom allow more possibilities as shown in Figure 5.2 for methane + CO_2 at 5 MPa.

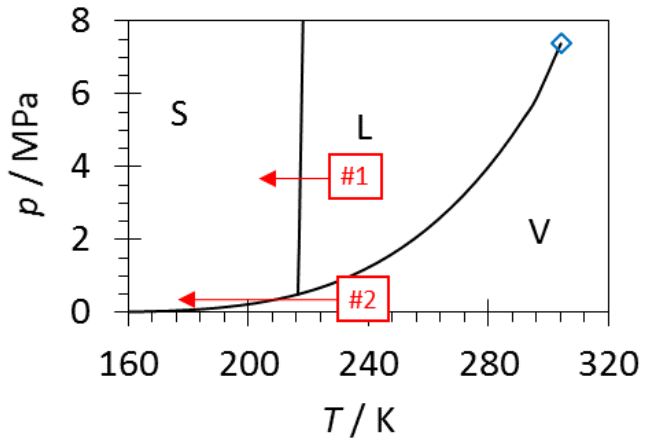

Figure 5.1. Pressure-temperature phase diagram for pure carbon dioxide, where V = Vapour, L = Liquid, S = Solid, and the number, #, in the red box refers to the transition given in Table 5.1.

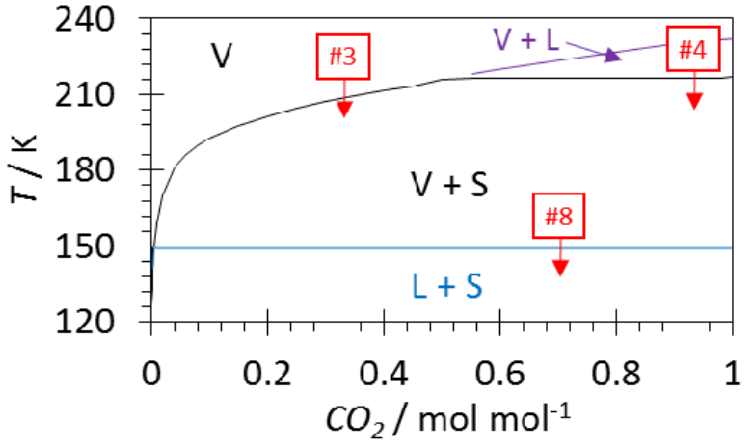

Figure 5.2: Temperature-composition phase diagram for the system methane and carbon dioxide (CO_2) at 5 MPa, where V = vapour, L = Liquid, S = Solid and the number, #, in the red box refers to the transition number as given in Table 5.1.

For example, if temperature is reduced along a pathway of constant pressure (5 MPa) and composition z_{CO2} = 0.2 a solid phase will first appear as part of a vapour to vapour + solid transition (#3) at around 200 K (see Figure 5.2). Further cooling along this path will produce a transition (#8) where the vapour + solid equilibrium becomes a liquid + solid equilibrium.

Table 5.1 presents the Baker-May classification of transition pathways related to solid equilibrium that were identified using ThermoFAST. The classification also indicates whether each transition pathway can be the highest solid equilibrium temperature (HSET) and/or occur at a temperature below the HSET. Some of these transition pathways are only possible in multi-component mixtures as a consequence of Gibbs Phase rule. Correctly identifying which type of transition is associated with the appearance of a solid phase at a given condition is important in an LNG production context because processing in upstream operations can in principle produce a fluid mixture containing no solids that is initially at a condition below its HSET.

Table 5.1: The Baker-May classification of transition pathways involving solid equilibrium for pure fluids and mixtures. The ability for the transition to be the highest solid equilibrium temperature (HSET) and/or occur at a temperature below HSET is also indicated.

Path	Can be HSET?	Can be below HSET?	Description of Transition
			Pure Fluids Only[#]
#1	True	False	Liquid to Solid*
#2	True	False	Vapour to Solid*
			Multicomponent Mixtures (≥ 2 components)
#3	True	False	Vapour to SVE
#4	True	False	VLE to SVE
#5	True	True	Liquid to SLE
#6	True	False	Liquid to SLE (Liquid Retrograde)
#7	False	True	SLE (Liquid Retrograde) to SVE (SLVE)
#8	False	True	SVE to SLE (SLVE)
#9	False	True	SVE to SLE (Solid Retrograde)
#10	False	True	SLE (Solid Retrograde) to SLE (Normal)^
#11	False	True	SVE to SVE (Solid Retrograde)^
#12	False	True	SVE to VLE (SLVE) [or SVE (Solid Retrograde) to VLE]
#13	False	True	VLE to Liquid
#14	False	True	SLE (Solid Retrograde) to Liquid
#15	False	True	SVE to Liquid [or SVE (Solid Retrograde) to Liquid]^
			Multicomponent Mixtures (≥ 3 components)
#16	True	False	VLE to SLVE (Liquid Retrograde)
#17	True	False	VLE to SLVE
#18	False	True	SLE (Liquid Retrograde) to SLVE
#19	False	True	SLE (Liquid Retrograde) to SLVE (Liquid Retrograde)
#20	False	True	SLVE (Liquid Retrograde) to SVE
#21	False	True	SLVE to SLE (Solid Retrograde)
#22	False	True	SLVE to SLE
#23	False	True	SVE to SLVE
#24	False	True	SVE to SLVE (Solid Retrograde)
#25	False	True	SLVE (Solid Retrograde) to Liquid
#26	False	True	SLVE (Solid Retrograde) to VLE

Binary mixtures at their Eutectic compositions can also undergo these transitions

* the special case of a pathway that passes through the pure fluid's triple point is considered an intersecting subset of pathway #1 and #2

^ Pathways are not phase transitions since no new phase appears. They are termed "retrograde-only transitions" as they correspond to the location of either a minimum or a maximum in the amount of solid phase with decreasing temperature.

5.1 Retrograde Solidification

The term retrograde is used frequently in Table 5.1 and refers to a decrease in the amount of a given phase with decreasing temperature, in contrast to normal behaviour, where the amount of that phase would otherwise increase as the temperature is lowered. This is conceptually similar to retrograde condensation [38]. For example, the normal behaviour of a solid-liquid system is to increase the amount of solid as the temperature decreases; however, in mixtures a retrograde behaviour can be found where the amount of solid present decreases as the temperature is lowered. As a conceptual example, consider a mixture at equilibrium with vapour, liquid and solid phases initially present. Upon cooling, as components in the vapour phase begin to liquefy there could be more solvent (or liquid) to help re-dissolve the solute back into solution, thus producing retrograde behaviour of the solid.

Solid retrograde behaviour is also possible in the absence of a vapour phase. Consider the isobaric cooling of a solid-liquid system where the normal behaviour of forming additional solid would cause the remaining liquid to become excessively volatile for the system pressure. Increasing the amount of solid with cooling (i.e. normal behaviour) would then require a more extreme type of retrograde behaviour, namely the formation of a vapour phase with a reduction in temperature. Such a system would likely be unstable as the remaining, richer liquid could re-dissolve the solid, and then the heavy liquid could absorb some of the vapour phase. Rather than allow the formation of a vapour phase upon a reduction in temperature, the solid phase instead redissolves in such systems, exhibiting solid retrograde behaviour.

5.2 Exemplar Transitions in Mixtures with Benzene

Descriptions and examples for all of the transition pathways listed in Table 5.1 are provided through ThermoFAST's Help function, in the software package's User Manual, and also in Baker (2018) [29]. Many of them can be illustrated via examples of binary and multi-component mixtures in which benzene is a solute. Figure 5.3 shows temperature composition phase diagrams for the methane + benzene binary mixture at a constant pressure of 5.41 MPa. At this pressure, the binary mixture exhibits 11 separate transition pathways, including the onset of retrograde solidification behaviour at around 200 K for benzene mole fractions larger than 10^{-4} (#9). At around 180 K, this retrograde behaviour reverts to normal solidification as the amount of solid phase present passes through a minimum at this transition pathway (#10).

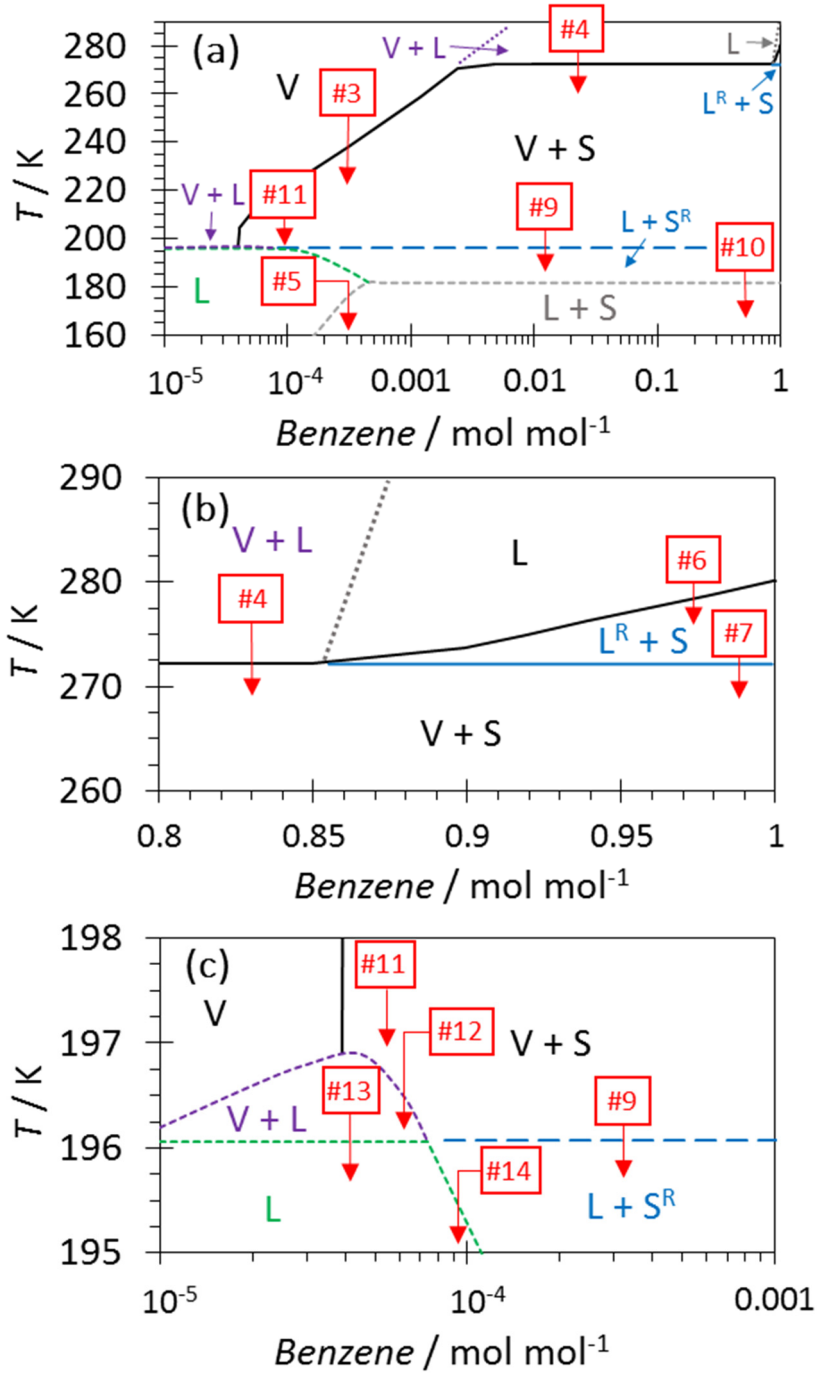

Figure 5.3: Temperature-composition phase diagram for the system methane and benzene at 5.41 MPa, where V = vapour, L = liquid, and S = solid. The superscript R indicates that the phase exhibits retrograde behaviour (amount decreases with decreasing temperature) and the number, #, in the red box refers to the transition number as given in Table 5.1. Figure (b) and Figure (c) are subsets of Figure (a).

Figure 5.4 shows temperature composition phase diagrams for a ternary mixture of benzene in a methane + propane solvent at a constant pressure of 5 MPa. Figure 5.5 shows temperature composition phase diagrams for benzene in multi-component solvent at 1.2 MPa. These systems contain further examples of unusual transition pathways, such as the onset of

retrograde solidification upon cooling from a SLVE to an SLE condition (#21), and the complete disappearance of a solid phase upon cooling from an SLVE to a VLE condition (#26).

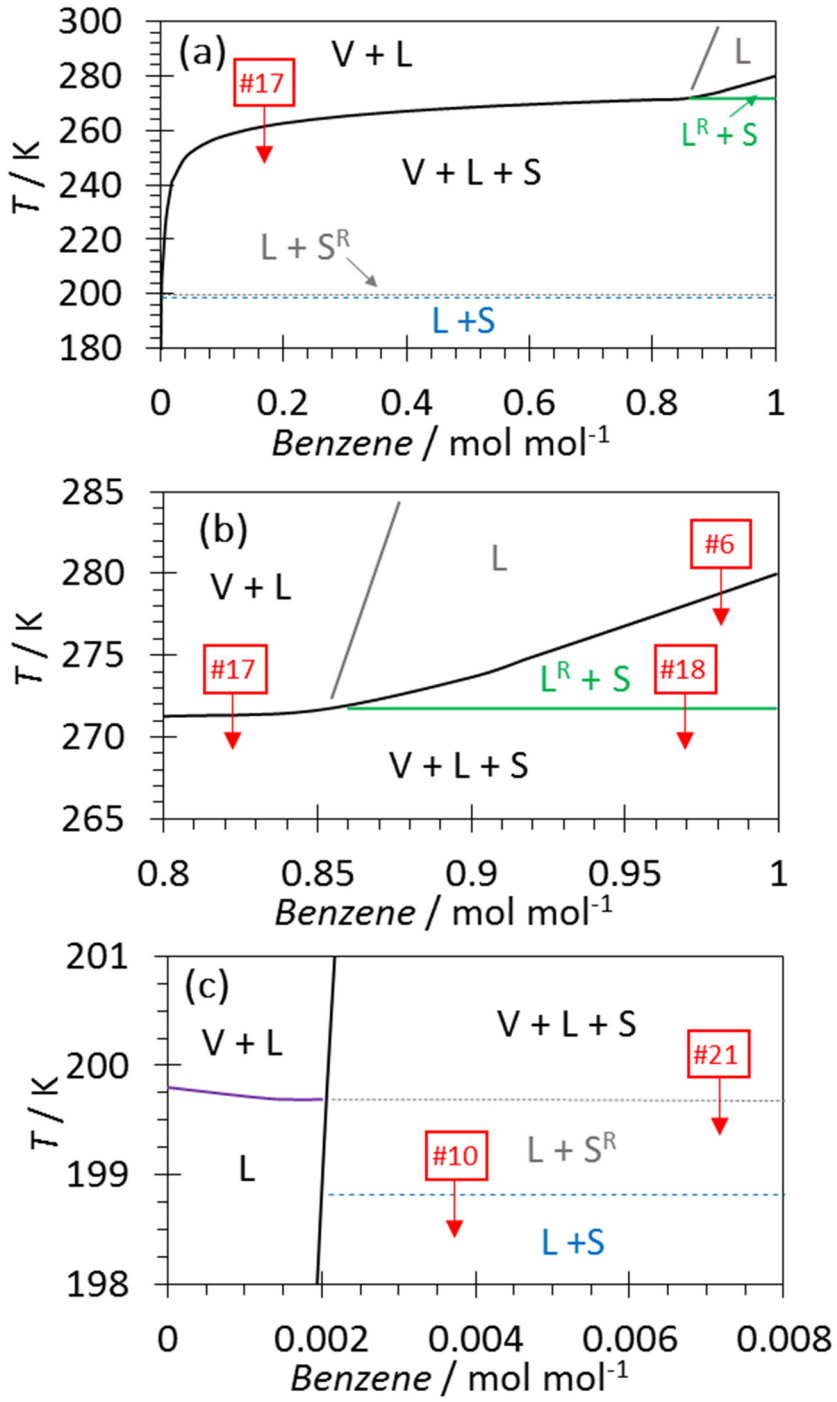

Figure 5.4: Temperature-composition phase diagram for the system methane, propane and benzene at 5 MPa (excluding benzene, the solvent's composition is 0.909 CH_4 + 0.091 C_3H_8), where V = vapour, L = liquid, and S = solid. The superscript R indicates that the phase exhibits retrograde behaviour (amount decreases with decreasing temperature) and the number, #, in the red box refers to the transition number as given in Table 5.1. Figure (b) and Figure (c) are subsets of Figure (a).

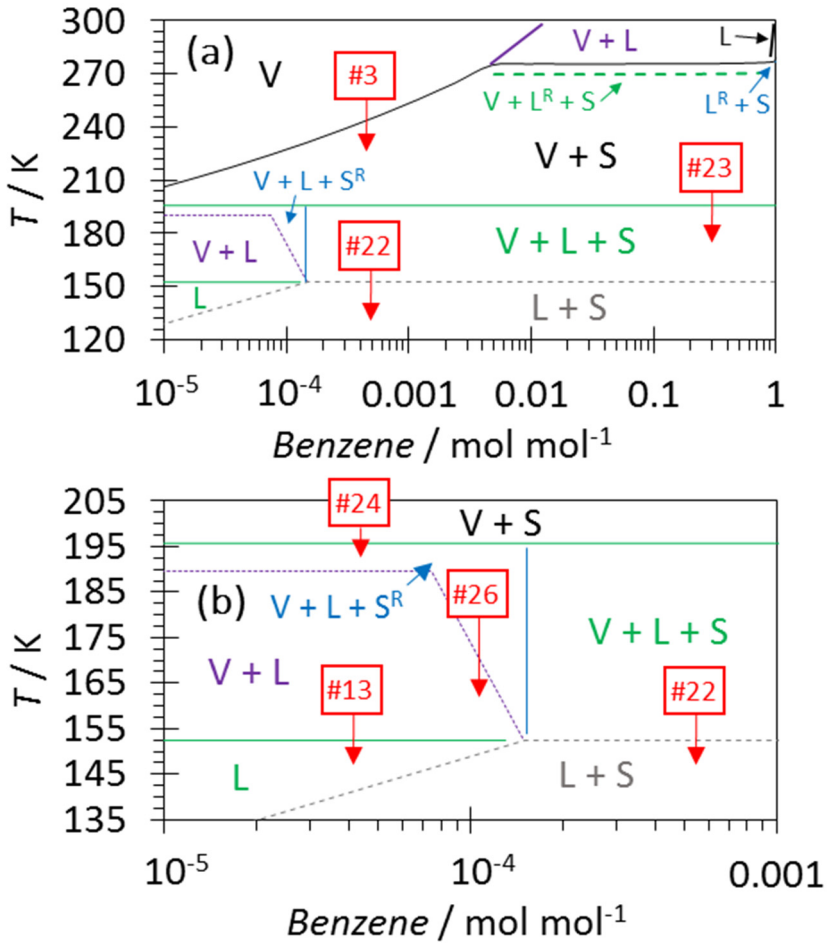

Figure 5.5: Temperature-composition phase diagram for the system nitrogen, methane, ethane, propane and benzene at 1.2 MPa (excluding benzene, the solvent's composition is 0.015 N_2 + 0.915 CH_4 + 0.06 C_2H_6 + 0.01 C_3H_8), where V = vapour, L = liquid, and S = solid. The superscript R indicates that the phase exhibits retrograde behaviour (amount decreases with decreasing temperature) and the number, #, in the red box refers to the transition number as given in Table 5.1. Figure (b) is a subset of Figure (a).

6 Conclusions

The thermodynamic calculator, ThermoFAST, has been optimised to represent the available data for heavy hydrocarbon solubility over a wider range of components and conditions than the KLSSP software tool. ThermoFAST showed a root-mean-squared deviation to experimental data of only 1.1 K at low concentrations of heavy compounds, which represents a 5-fold improvement over KLSSP. The introduction of the Baker-May classification of transition pathways involving solid equilibrium located 26 phase transitions including SVE, SLE and SLVE which ThermoFAST was able to predict due to the underlying thermodynamic model based on the PR EOS and an equation for calculating pure solid fugacities.

Research programs are currently underway in the Fluid Science and Resources Division at the University of Western Australia to produce new experimental data for the solubility of various compounds in hydrocarbon solvents. These new data sets will be used to extend the predictive capabilities of ThermoFAST; we anticipate that, in collaboration with the GPA Midstream Association's Research Committee, new versions of ThermoFAST which incorporate these improvements will be released in the future.

7 References

1. Saadawi, H. *Global Natural Gas Outlook*. 2018 Ringstone Petroleum [Accessed: 08 / 02 / 2018]; Available from: https://www.spe.org/en/ogf/ogf-article-detail/?art=3762.
2. *BP Energy Outlook*. 2017 BP p.l.c. [Accessed: 08 / 02 / 2018]; Available from: https://www.bp.com/content/dam/bp/pdf/energy-economics/energy-outlook-2017/bp-energy-outlook-2017.pdf.
3. Baker, C.J., Oakley, J.H., Rowland, D., Hughes, T.J., Aman, Z.M. and May, E.F., *Rapid Simulation of Solid Deposition in Cryogenic Heat Exchangers To Improve Risk Management in Liquefied Natural Gas Production.* Energy Fuels, 2018(32): p. 255-267 DOI: http://doi.org/10.1021/acs.energyfuels.7b03057.
4. Kohn, J.P., Luks, K.D. and Liu, P.H., *Three-phase solid-liquid-vapor equilibriums of binary-n-alkane systems (ethane-n-octane, ethane-n-decane, ethane-n-dodecane).* J. Chem. Eng. Data, 1976. **21**(3): p. 360-362 DOI: http://doi.org/10.1021/je60070a012.
5. Kohn, J.P., Luks, K.D., Liu, P.H. and Tiffin, D.L., *Three-phase solid-liquid-vapor equilibriums of the binary hydrocarbon systems methane-n-octane and methane-cyclohexane.* J. Chem. Eng. Data, 1977. **22**(4): p. 419-421 DOI: http://doi.org/10.1021/je60075a011.
6. Liu, P.H., Luks, K.D. and Kohn, J.P., *Three-phase solid-liquid-vapor equilibria of the systems ethane-benzene, ethane-cyclohexane, and ethane-trans-decalin.* J. Chem. Eng. Data, 1977. **22**(2): p. 220-221 DOI: http://doi.org/10.1021/je60073a014.
7. Tiffin, D.L., Kohn, J.P. and Luks, K.D., *Three-phase solid-liquid-vapor equilibriums of binary ethylene-n-alkane systems (ethylene-n-octane, ethylene-n-decane, ethylene-n-dodecane).* J. Chem. Eng. Data, 1978. **23**(3): p. 207-209 DOI: https://doi.org/10.1021/je60078a013.
8. Tiffin, D.L., Kohn, J.P. and Luks, K.D., *Solid hydrocarbon solubility in liquid methane-ethane mixtures along three-phase solid-liquid-vapor loci.* J. Chem. Eng. Data, 1979. **24**(4): p. 306-310 DOI: http://doi.org/10.1021/je60083a013.
9. Tiffin, D.L., Kohn, J.P. and Luks, K.D., *Three-phase solid-liquid-vapor equilibriums of the systems ethylene-cyclohexane, ethylene-trans-decalin, ethylene-benzene, and ethylene-2-methylnaphthalene.* J. Chem. Eng. Data, 1979. **24**(2): p. 96-98 DOI: http://doi.org/10.1021/je60081a019.
10. Tiffin, D.L., Kohn, J.P. and Luks, K.D., *Three phase solid-liquid-vapor equilibriums of the binary hydrocarbon systems ethane-2-methylnaphthalene, ethane-naphthalene, propane-n-decane, and propane-n-dodecane.* J. Chem. Eng. Data, 1979. **24**(2): p. 98-100 DOI: http://doi.org/10.1021/je60081a020.
11. Chen, W.-L., Callahan, S.F., Luks, K.D. and Kohn, J.P., *Effect of the presence of nitrogen on solid solubility of normal paraffins in liquid methane.* J. Chem. Eng. Data, 1981. **26**(2): p. 166-168 DOI: http://doi.org/10.1021/je00024a022.
12. Chen, W.-L., Luks, K.D. and Kohn, J.P., *Three-phase solid-liquid-vapor equilibriums of the binary hydrocarbon systems propane-benzene, propane-cyclohexane, butane-benzene, butane-cyclohexane, butane-n-decane, and butane-n-dodecane.* J. Chem. Eng. Data, 1981. **26**(3): p. 310-312 DOI: http://doi.org/10.1021/je00025a027.
13. Hottovy, J.D., Kohn, J.P. and Luks, K.D., *Partial miscibility behavior of the methane-ethane-n-octane system.* J. Chem. Eng. Data, 1981. **26**(2): p. 135-137 DOI: http://doi.org/10.1021/je00024a009.

14. Luks, K.D., Hottovy, J.D. and Kohn, J.P., *Three-phase solid-liquid-vapor equilibriums in the binary hydrocarbon systems methane-n-hexane and methane-benzene.* J. Chem. Eng. Data, 1981. **26**(4): p. 402-403 DOI: http://doi.org/10.1021/je00026a016.
15. Hottovy, J.D., Kohn, J.P. and Luks, K.D., *Partial miscibility behavior of the ternary systems methane-propane-n-octane, methane-n-butane-n-octane, and methane-carbon dioxide-n-octane.* J. Chem. Eng. Data, 1982. **27**(3): p. 298-302 DOI: http://doi.org/10.1021/je00029a020.
16. Luks, K.D., Kohn, J.P., Liu, P.H. and Kulkarni, A.A., *Solubility of hydrocarbons in cryogenic NGL and LNG.* GPA RR-033, 1975.
17. Kohn, J.P. and Luks, K.D., *Solubility of Hydrocarbons in Cryogenic LNG and NGL Mixtures.* GPA RR-022, 1976.
18. Jasperson, L.V., Mcdougal, R.J. and Wilson, G.M., *Equilibrium Data (SLE and VLE) for Heavy and Light Hydrocarbons at Cryogenic Temperatures.* Wiltec Research Co., Inc., Provo, Utah, GPA RR-215 Project 035, 2014.
19. Gupta, A.K., Bishnoi, R.P. and Kalogerakis, N., *A method for the simultaneous phase equilibria and stability calculations for multiphase reacting and non-reacting systems.* Fluid Phase Equilib., 1991. **63**(1): p. 65-89 DOI: https://doi.org/10.1016/0378-3812(91)80021-M.
20. Ballard, A.L.S., E.D., *The next generation of hydrate prediction: Part III. Gibbs energy minimisation formalism.* Fluid Phase Equilib., 2004. **218**(1): p. 15-31.
21. Peng, D.-Y. and Robinson, D.B., *A New Two-Constant Equation of State.* Ind. Eng. Chem., 1976. **15**(1): p. 59-64.
22. Hildebrand, J.H. and Scott, R.L., *The Solubility of Nonelectrolytes*. 1950, New York: Reinhold Pub. Corp.
23. Prausnitz, J.M., Lichtenthaler, R.N. and De Azevedo, E.G., *Molecular Thermodynamics of Fluid-Phase Equilibria*. 1998: Pearson Education.
24. Brown, T.S., Niesen, V.G., Erickson, D.D. and Inc., C., *The Effects of Light Ends and High Pressure on Paraffin Formation.* Soc. Pet. Eng. J., 1994. **28505**.
25. Lira-Galeana, C., Firoozabadi, A. and Prausnitz, J.M., *Thermodynamics of wax precipitation in petroleum mixtures.* AIChE J., 1996. **42**(1): p. 239-248 DOI: http://doi.org/10.1002/aic.690420120.
26. Morgan, D.L. and Kobayashi, R., *Triple point corresponding states in long-chain n-alkanes.* Fluid Phase Equilib., 1991. **63**(3): p. 317-327 DOI: https://doi.org/10.1016/0378-3812(91)80038-W.
27. Won, K.W., *Thermodynamics for solid solution-liquid-vapor equilibria: wax phase formation from heavy hydrocarbon mixtures.* Fluid Phase Equilib., 1986. **30**(Supplement C): p. 265-279 DOI: https://doi.org/10.1016/0378-3812(86)80061-9.
28. Assael, M.J., Trusler, J.M. and Tsolakis, T.F., *Thermophysical Properties of Fluids: An Introduction to Their Prediction.* 1996.
29. Baker, C.J., *Phase Equilibrium Measurements and Advanced Modelling for Optimising Liquefied Natural Gas Production.* PhD Thesis, The University of Western Australia, 2018.
30. Pikaar, M.J., *A study of phase equilibria in hydrocarbon-CO_2 systems* Ph.D. Thesis, Imperial College London 1959.
31. Kuebler, G.P. and Mckinley, C., *Solubility of solid benzene, toluene, n-hexane and n-heptane in liquid methane.* Adv. Cryog. Eng., 1974. **9**: p. 320.
32. Rijkers, M.P.W.M., Hathie, M., Peters, C.J. and De Swaan Arons, J., *Experimental determination of the phase behavior of binary mixtures of methane + benzene: Part II.*

The solubility of liquid benzene in supercritical methane. Fluid Phase Equilib., 1992. **77**(Supplement C): p. 343-353 DOI: http://doi.org/10.1016/0378-3812(92)85113-M.
33. Siahvashi, A., Al-Ghafri, S.Z.S., Hughes, T.J., Graham, B.F., Huang, S.H. and May, E.F., *Solubility of p-Xylene in Methane and Ethane.* In Preparation, 2018.
34. Preston, G.T., Funk, E.W. and Prausnitz, J.M., *Solubilities of hydrocarbons and carbon dioxide in liquid methane and in liquid argon.* J. Phys. Chem. B, 1971. **75**(15): p. 2345-2352 DOI: http://doi.org/10.1021/j100684a020.
35. Zhang, J., Sun, J., Zhang, X., Zhao, Y. and Zhang, S., *The recent development of CO2 fixation and conversion by ionic liquid.* Greenh Gases, 2011. **1**(2): p. 142-159 DOI: http://doi.org/10.1002/ghg.13.
36. Shen, W., He, Y., Zhang, S., Li, J. and Fan, W., *Yeast-Based Microporous Carbon Materials for Carbon Dioxide Capture.* ChemSusChem, 2012. **5**(7): p. 1274-1279 DOI: http://doi.org/10.1002/cssc.201100735.
37. Le, T.T. and Trebble, M.A., *Measurement of Carbon Dioxide Freezing in Mixtures of Methane, Ethane, and Nitrogen in the Solid−Vapor Equilibrium Region.* J. Chem. Eng. Data, 2007. **52**(3): p. 683-686 DOI: http://doi.org/10.1021/je060194j.
38. Katz, D.L. and Kurata, F., *Retrograde Condensation.* Ind. Eng. Chem., 1940. **32**(6): p. 817-827 DOI: http://doi.org/10.1021/ie50366a018.

8 Appendices

See below.

8.1 Appendix A: Individual deviations to solid equilibrium data for all mixtures

Table 8.1: Summary of the root-mean-squared deviations (rmsd) of ThermoFAST predictions from available solid equilibrium literature data for all systems covered by ThermoFAST. Different colours have the following meanings: yellow = tuned; green = limited data or quality is not adequate; blank = no data available; black = binary already described. Abbreviations have the following meanings: cyc = cyclo, me = methyl, Et = ethyl, Bz = benzene, Tol = toluene and Xy = xylene.

ThermoFAST T_{rmsd} / K	CO_2	C_1	C_2	C_3	iC_4	nC_4	iC_5	nC_5	Neo-C_5	Cyc-C_5	Me-Cyc-C_5	nC_6	cyc-C_6	nC_7	nC_8	nC_9	nC_{10}	Bz	Tol	Et-Bz	m-Xy	o-Xy	p-Xy
CO_2																							
C_1	2.06																						
C_2	1.40																						
C_3	2.04																						
iC_4																							
C_4	1.96	0.50																					
iC_5																							
C_5		0.37					3.24																
neo-C_5		3.31																					
cyc-C_5		5.36																					
me-cyc-C_5		1.23																					
nC_6		0.80	0.24				1.23																
cyc-C_6		1.76	5.28	3.45		7.59						3.96											
nC_7		0.59	0.52																				
nC_8		0.25	1.64									0.71	0.37	0.77									
nC_9		0.97																					
nC_{10}		0.06	0.31	0.39		0.40								1.08	0.95								
Bz		1.63	2.16	0.84		2.15						2.86	3.74	1.09	0.88								
Tol		1.39		0.64									2.78	0.15				5.47					
Et-Bz														0.15				2.25	0.69				
m-Xy																		1.55	2.35				
o-Xy																		0.27	1.10		1.25		
p-Xy		0.70	2.68															0.54	1.81	0.84	1.88	1.16	

Table 8.2: Summary of the root-mean-squared deviations (rmsd) of KLSSP predictions from available solid equilibrium literature data for all systems covered by ThermoFAST. Different colours have the following meanings: yellow = tuned; green = limited data or quality is not adequate; blank = no data available; black = binary already described; dark gray = not available in KLSSP. Abbreviations have the following meanings: cyc = cyclo, me = methyl, Et = ethyl, Bz = benzene, Tol = toluene and Xy = xylene.

KLSSP T_{rmsd} / K	CO_2	C_1	C_2	C_3	iC_4	nC_4	iC_5	nC_5	neo-C_5	cyc-C_5	me-Cyc-C_5	nC_6	cyc-C_6	nC_7	nC_8	nC_9	nC_{10}	Bz	Tol	Et-Bz	m-Xy	o-Xy	p-Xy
CO_2																							
C_1	19.52																						
C_2	38.42																						
C_3	37.40																						
iC_4																							
nC_4	16.33	7.77																					
iC_5																							
nC_5		2.30					4.24																
neo-C_5																							
cyc-C_5																							
me-Cyc-C_5																							
nC_6		19.46	8.11				7.15																
Cyc-C_6		33.74	64.01	55.05		43.25						59.06											
nC_7		39.13	0.47																				
nC_8		8.63	18.11									6.27	47.52	3.08									
nC_9		11.11																					
nC_{10}		1.97	0.72	1.38		1.46								9.00	3.50								
Bz		7.76	5.40	3.64		3.41						20.47	47.13	30.62	16.57								
Tol																							
Et-Bz																							
m-Xy																							
o-Xy																							
p-Xy																							

Table 8.3: Summary of the root-mean-squared deviations (rmsd) of (a) ThermoFAST and (b) KLSSP predictions from available solid equilibrium literature data for all systems covered by KLSSP (see Table 1.1 Different colours have the following meanings: yellow = tuned; green = limited data or quality is not adequate; orange; data available but not within the recommended range of KLSSP; blank = no data available; black = binary already described; dark gray = not available in KLSSP. Abbreviations have the following meanings: cyc = cyclo, me = methyl, Et = ethyl, Bz = benzene, Tol = toluene and Xy = xylene.

(a) T_{rmsd} / K ThermoFAST	CO_2	C_1	C_2	C_3	iC_4	nC_4	iC_5	nC_5	nC_6	cyc-C_6	nC_7	nC_8	nC_9	nC_{10}	Bz
CO_2															
C_1	2.2														
C_2	0.9														
C_3	1.5														
iC_4															
nC_4		0.8													
iC_5															
nC_5		0.4													
nC_6		0.9	0.2												
cyc-C_6		0.5													
nC_7		0.6	0.5												
nC_8		0.3	0.3												
nC_9		1.2													
nC_{10}			1.3	0.4											
Bz		1.5	5.2												

(b) T_{rmsd} / K KLSSP	CO_2	C_1	C_2	C_3	iC_4	nC_4	iC_5	nC_5	nC_6	cyc-C_6	nC_7	nC_8	nC_9	nC_{10}	Bz
CO_2															
C_1	16.4														
C_2	2.8														
C_3	3.7														
iC_4															
nC_4		2.7													
iC_5															
nC_5		2.4													
nC_6		3.6	8.1												
cyc-C_6		10.4													
nC_7		1.9	0.5												
nC_8		9.5	1.2												
nC_9		16.2													
nC_{10}			0.7	1.5											
Bz		8.4	4.8												